SLD Physics Note 54
October 1, 1996

Measurement of the Tau Lorentz Structure with Polarized Beams

N. Allen, M. Daoudi, E. Etzion, J. Johnson, A. McKemey, J. Quigley

Abstract

We present a new measurement of the tau neutrino helicity (h_{ν_τ}) and the Michel parameters (ρ, ξ and δ). The measurement exploits the highly polarized SLC electron beam to extract these physics quantities from a direct measurement of the τ decay spectra. The analysis uses the 1993-1995 SLD data sample of 4316 $e^+e^- \rightarrow Z^0 \rightarrow \tau^+\tau^-$ events. By analyzing the τ decays $\tau \rightarrow \pi(K)\nu_\tau$, $\tau \rightarrow \rho\nu_\tau$ we obtain preliminary results of $h_{\nu_\tau} = -0.97 \pm 0.10 \pm 0.04$. The leptonic decay channels $\tau \rightarrow e\bar{\nu}_e\nu_\tau$ and $\tau \rightarrow \mu\bar{\nu}_\mu\nu_\tau$ yield the preliminary results: $\rho = 0.71 \pm 0.09 \pm 0.05$, $\xi = 1.03 \pm 0.36 \pm 0.05$ and $\xi\delta = 0.84 \pm 0.27 \pm 0.05$.

1 Introduction

The weak couplings of the tau may be studied by investigating the energy spectra of various tau decay products. These spectra are determined by the spin polarization of the taus and the nature of the decay [1].

At the Z^0 , taus are produced with spin polarization due to the inherent parity violation of the Z^0 couplings. At the SLC, this is enhanced due to the electron beam polarization [2]. We can write the production cross sections for left and right handed taus as follows:

$$\begin{aligned}
\frac{1}{\sigma_{tot}}\frac{d\sigma_L}{d\cos\theta} &= \tfrac{3}{16}(1+\mathrm{A}_\tau)[(1-\mathrm{A}_e P_e)(1+\cos^2\theta)+2(\mathrm{A}_e-P_e)\cos\theta], \\
\frac{1}{\sigma_{tot}}\frac{d\sigma_R}{d\cos\theta} &= \tfrac{3}{16}(1-\mathrm{A}_\tau)[(1-\mathrm{A}_e P_e)(1+\cos^2\theta)-2(\mathrm{A}_e-P_e)\cos\theta], \qquad (1)
\end{aligned}$$

where θ is the polar angle of the τ^- (τ^+) with respect to the incident electron (positron) direction, P_e is the electron beam polarization, and A_e and A_τ are the electron and tau parity-violation asymmetry parameters defined as:

$$\mathrm{A}_\ell = \frac{2\hat{g}_v^\ell/\hat{g}_a^\ell}{1+(\hat{g}_v^\ell/\hat{g}_a^\ell)^2}, \qquad (2)$$

where $\hat{g}_v^\ell/\hat{g}_a^\ell$ is the ratio between the effective Z^0 vector and axial-vector couplings to the leptons.

This results in the following expression for the tau polarization as a function of angle and beam polarization:

$$P_\tau(\cos\theta, P_e) = \frac{\frac{d\sigma_R}{d\cos\theta}-\frac{d\sigma_L}{d\cos\theta}}{\frac{d\sigma_R}{d\cos\theta}+\frac{d\sigma_L}{d\cos\theta}} = -\frac{\mathrm{A}_\tau + 2\frac{\mathrm{A}_e-P_e}{1-\mathrm{A}_e P_e}\frac{\cos\theta}{1+\cos^2\theta}}{1+2\mathrm{A}_\tau\frac{\mathrm{A}_e-P_e}{1-\mathrm{A}_e P_e}\frac{\cos\theta}{1+\cos^2\theta}}. \qquad (3)$$

Due to the large beam polarization at SLC, tau polarizations are much higher than at LEP, especially at high $|\cos\theta|$ (see Fig. 1). Also, the polarization of the tau is largely determined by the beam polarization and the production angle, and is relatively unaffected by the Z^0 parity violation.

In this paper, we study the energy spectra of taus decaying to pions, rho mesons, electrons and muons. In the case of a two body decay, such as $\tau\rightarrow\pi(\mathrm{K})\nu_\tau$ or $\tau\rightarrow\rho\nu_\tau$, the decay spectrum at rest is mono-energetic, so the boosted energy spectrum directly reflects the production angle of the pion or rho meson in the rest frame. In the case of a three body decay, such as $\tau\rightarrow\mu\bar{\nu}_\mu\nu_\tau$ or $\tau\rightarrow e\bar{\nu}_e\nu_\tau$, the boosted energy spectrum is a combination of both the rest frame angular distribution and energy spectra. In all of these cases, we can parameterize the decay spectrum in two parts, a constant part that is unaffected by the handedness of the tau, and a polarization- dependent part that changes sign depending on

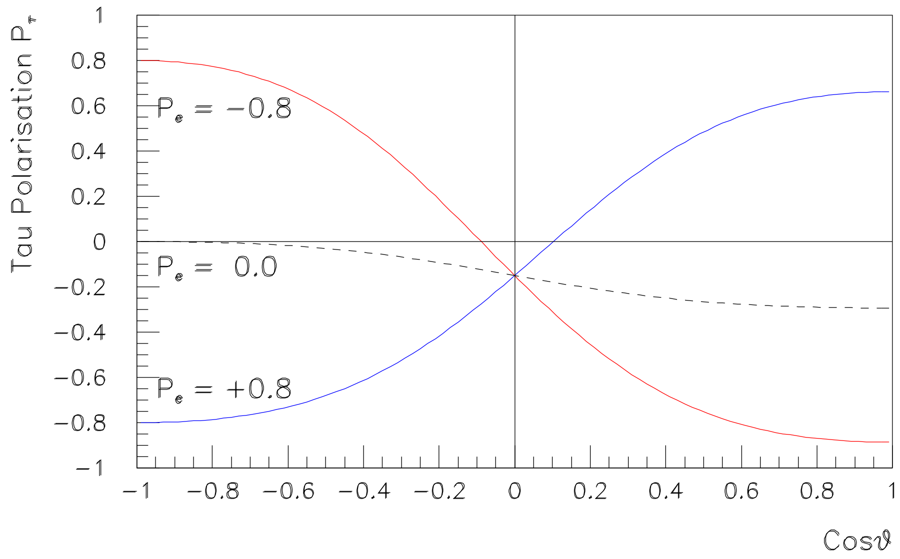

Figure 1: Tau polarization vs production angle with and without beam polarization.

the handedness of the tau:

$$\frac{1}{\Gamma}\frac{d\Gamma_L}{dz} = f(z) + g(z),$$
$$\frac{1}{\Gamma}\frac{d\Gamma_R}{dz} = f(z) - g(z). \tag{4}$$

For the hadronic modes the decay distribution can alternatively be written in the generic form:

$$\frac{1}{\Gamma}\frac{d\Gamma}{dz} = f(z) + \mathrm{h}_{\nu_\tau} g(z), \tag{5}$$

where h_{ν_τ} characterizes the polarization dependent term. For the $\tau \rightarrow \pi(\mathrm{K})\nu_\tau$ mode, z is the hadron's energy scaled by the τ energy ($z = \frac{E_h}{E_T}$), and f(z) and g(z) are:

$$\begin{aligned} f(z) &= 1, \\ g(z) &= \frac{2z - 1 - m_h^2/m_\tau^2}{1 - m_h^2/m_\tau^2}. \end{aligned} \tag{6}$$

For the $\tau \rightarrow \rho\nu_\tau$ decay mode, it is necessary to spin analyze the decay products of the ρ, as discussed in [3, 4], otherwise sensitivity would be lost. Hence, z represents a set of three variables, the production angle of the ρ in the τ rest frame, θ^*, the production angle of the charged pion in the ρ rest frame, ψ, and the mass of the rho meson, m_ρ. However, since Eq. 5 has a linear dependence on the tau neutrino helicity it is useful to use the notation ω, introduced in Ref. [5]. The function $\omega(z)$ is the ratio between the polarization dependent term and the polarization-independent term

$$\omega(z) = \frac{g(z)}{f(z)}. \tag{7}$$

Taking this approach, all the hadronic tau decay distributions can be expressed in the same way:

$$\frac{1}{\Gamma}\frac{d\Gamma}{d\omega} = (1 + \mathrm{h}_{\nu_\tau}\omega(z)), \tag{8}$$

which allows a simultaneous fit to the $\tau \rightarrow \pi(\mathrm{K})\nu_\tau$ and $\tau \rightarrow \rho\nu_\tau$ decay modes.

In the case of the leptons, neglecting mass differences, we can describe the energy spectrum with the three Michel parameters[1] ρ, ξ and δ. Here the parameter ρ describes the polarization-independent term, and ξ and δ describe the polarization dependent terms. We get the following spectrum for $\tau \rightarrow \ell\bar{\nu}_\ell\nu_\tau$:

$$\begin{aligned} f(z) &= f_1 + \rho \cdot f_2, \\ g(z) &= \xi(g_1 + \delta \cdot g_2), \end{aligned} \tag{9}$$

where

$$\begin{aligned} f_1 &= 2 - 6z^2 + 4z^3, \\ f_2 &= \frac{4}{9}(-1 + 9z^2 - 8z^3), \\ g_1 &= -\frac{2}{3} + 4z - 6z^2 + \frac{8}{3}z^3, \quad \text{and} \\ g_2 &= \frac{4}{9}(1 - 12z + 27z^2 - 16z^3)]. \end{aligned} \tag{10}$$

Here $z = \frac{E_\ell}{E_\mathcal{T}}$.

These decay spectra are combined with the production cross sections to get theoretical decay distributions which can be written as:

$$\frac{1}{\sigma}\frac{d^2\sigma(z, \cos\theta, P_e)}{dz d\cos\theta} = f(z) - P_\mathcal{T}(\cos\theta, P_e) \cdot g(z), \tag{11}$$

which clearly illustrates the importance of high tau polarization for measuring the polarization dependent terms. For τ^+ decays, the sign of the polarization dependent term is reversed due the opposite helicity of the anti-neutrino. However, since at the Z^0 taus are produced in pairs with opposite helicities, if the τ^- direction is used as the lab frame variable the τ^- and τ^+ decay spectra are identical. This paper updates our previous preliminary results [8].

2 Apparatus

The results reported here are based on a sample of 4316 tau-pair candidates collected by the SLC Large Detector (SLD) during the period 1993-1995. The 1993 run accumulated

[1] These parameters were originally conceived to describe muon decay [6]. They describe the energy and the angular spectrum of the resultant electron with respect to the initial muon spin direction. Lepton universality implies that the tau Michel parameters should be identical to the well measured muon Michel parameters [7].

an integrated luminosity of 1.78 pb^{-1} with an average electron beam polarization of 63%, and the 1994-1995 run accumulated 3.66 pb^{-1} with an average polarization of 77%. A general description of the SLD can be found elsewhere [9]. Charged particle tracking and momentum analysis are provided by the Central Drift Chamber (CDC) [10] and the CCD-based vertex detector [11] in a uniform axial magnetic field of 0.6 T. Particle energies are measured in the Liquid Argon Calorimeter (LAC) [12], which is segmented into projective towers with separate electromagnetic and hadronic sections. The measured energy and the shape of the energy flow are used to distinguish between different particles. Additional particle identification is provided by a Čerenkov Ring-Imaging Detector (CRID) [13], and muons are identified and tracked in the Warm Iron Calorimeter (WIC) [14].

The SLD event trigger requires any of several combinations of tracking and energy-flow information from the detector elements. A subset of these have a relatively high efficiency for tau-pair events, in particular a requirement of at least two back-to-back tracks, or a single track plus a minimum energy deposition in the calorimeter.

3 Event Selection

The selection of tau-pair candidates at SLD (for details, see Ref. [15] and Appendix I) is based on the multiplicity, momentum and direction of tracks in the central drift chamber, and on properties of electromagnetic showers in the calorimeter. A sample of 4316 events were selected from the 1993-1995 data. The event selection efficiency and background contamination were estimated using Monte Carlo, and a detailed tabulation is given in Appendix I. The production of tau-pair events at the Z^0 resonance was simulated using the KORALZ4.0 [16] Monte Carlo generator. The same program was used to generate muon-pair events, while wide-angle Bhabha scattering, two-photon interactions, and multihadron final states were produced using the generators described in Refs. [17], [18], and [19], respectively. All these Monte Carlo data samples were subjected to the SLD detector simulation based on the GEANT3.21 [20] program, and to the above event selection. The SLD trigger was also simulated in the Monte Carlo.

Selected tau events are divided into hemispheres by the plane normal to the event thrust axis, and the hemispheres are treated independently. Any pairs of oppositely charged tracks which are consistent with originating from a photon conversion are removed, and hemispheres are then required to have only a single track.

For the selection of tau decays to single pions (or kaons), tracks are required to have no unassociated electromagnetic (EM) LAC energy clusters within 10° of the thrust axis. This requirement is powerful for rejecting backgrounds from decays into ρ or a_1. Electrons and muons are rejected by a series of hybrid cuts making use of information from the LAC and WIC. For the tracks that are left, the track momentum must be greater than 3 GeV/c and the total energy in the LAC divided by the track momentum must be less than 0.62. A further requirement of $E_{EM}/p < 0.42$ is made, and a quasi-invariant mass is calculated assuming that the associated cluster energy originated from photons and that the track is a pion. This quantity is required to be less than 0.3 GeV/c^2. Finally, due to the barrel WIC angular coverage, the remaining tracks are divided into two regions, namely $|\cos\theta| < 0.60$ and $0.60 < |\cos\theta| < 0.74$. The total energy in the LAC divided by the track momentum is required to be greater than 0.14 in the former and 0.31 in the latter case. These criteria discriminate effectively against muons. This selection provides a sample of 558 tracks identified as $\tau\rightarrow\pi(\mathrm{K})\nu_\tau$, with an efficiency of $57.9 \pm 0.4\%$ (within the angular acceptance) and a purity of approximately 79%. The selection efficiency and background are shown as a function of ω and $\cos\theta$ in Fig. 7. The non-tau background is estimated to be less than 0.5%.

τ Background	Percentage of Sample %
e	4.8±0.2
μ	1.4±0.1
ρ	12.9±0.4
Others	2.0±0.1
Total	21.1±0.5

Table 1: Tau background composition to selected $\tau\rightarrow\pi(\mathrm{K})\nu_\tau$ events.

Candidates for tau decays to rho mesons are selected by rejecting electrons and muons as described above and rejecting events selected as pion decays. Remaining events are categorized according to the number of calorimeter energy clusters found within 20° of the event thrust axis, and according to whether such clusters are associated or unassociated with the charged track in the corresponding hemisphere. Details are presented in Appendix I. Depending on the category, one of several sets of criteria must be met for a candidate to be accepted, and one of several methods is used to calculate a rho energy and invariant mass. Finally, all candidates are required to have a value of the calculated rho mass that falls in the range between 0.44 and 1.2 GeV/c^2. This selection results in a sample of 1295 identified rho decays in the 1993-1995 data, with an efficiency of $59.6 \pm 0.5\%$ (within an angular acceptance of $|\cos\theta| < 0.74$) and a purity of approximately 76%, as estimated from Monte Carlo studies. The non-tau background is estimated to be less than 0.3%. The selection efficiency and background are shown as a function of ω and $\cos\theta$ in Fig. 8.

τ Background	Percentage of Sample %
e+μ	0.8±0.1
π	2.2±0.1
$\pi 2\pi^0$	14.7±0.3
Others	5.9±0.2
Total	23.6±0.4

Table 2: Tau background composition to selected $\tau\rightarrow\rho\nu_\tau$ events.

For tau decays to muons, the sample is divided into polar angle regions as above, and tracks are required to have at least one hit in the VXD. In the region of $|\cos\theta| < 0.62$, the WIC is used to identify muons by associating WIC hits with CDC tracks. In the $0.62 < |\cos\theta| < 0.75$ region, shower information from the LAC is used instead. We require that E/p be less than 0.3, that the total number of electromagnetic LAC towers hit in the associated cluster be less than 4, and that there be no unassociated neutral clusters within 15° of the track. In addition, the quasi-invariant mass (calculated as above) is required to be less than 180 MeV/c^2. This results in a sample of 1123 tracks identified as muons, with an estimated selection efficiency of $69.0 \pm 0.3\%$ within the acceptance, and an estimated purity of 94%.

Background	Percentage of Sample %
τ	3.3±0.1
μ-pair	2.1±0.3
2γ	1.1±0.2
Total	6.4±0.4

Table 3: Background composition to selected $\tau\rightarrow\mu\bar{\nu}_\mu\nu_\tau$ events.

Criteria for selection of tau decays to electrons are the same over the full range $|\cos\theta| < 0.75$, and again one VXD hit is required on all tracks. The LAC shower shape must be consistent with that of an electron, or any valid CRID data must strongly favor the electron hypothesis over the pion hypothesis. We require that no energy be deposited in the back hadronic section of the LAC, and that between 3 and 25 electromagnetic LAC towers be hit in the associated cluster. In addition, if there are no unassociated neutral clusters within 15° of the track, we require that the quasi-invariant mass be less than 500 MeV/c^2. If there are one or two unassociated clusters within 15° of the track, we construct the invariant mass of the cone assuming the track is a pion and the clusters photons, and require this quantity to be less than 500 MeV/c^2. This results in a sample of 932 identified electron tracks with an estimated efficiency of $61.7 \pm 0.3\%$ within the acceptance and an estimated purity of 96%.

Background	Percentage of Sample %
τ	2.2±0.1
Bhabha	0.9±0.2
2γ	0.9±0.2
Total	4.0±0.3

Table 4: Background composition to selected $\tau\rightarrow e\bar{\nu}_e\nu_\tau$ events.

4 Data Analysis

As discussed in section 1, and shown in Fig. 1, the average τ polarization depends strongly on production angle and on the sign of the electron beam polarization. The large analyzing power that comes from the large SLC beam polarization is clearly demonstrated in Fig. 2, where the energy spectrum of $\tau \rightarrow \pi(\mathrm{K})\nu_\tau$ decays is plotted separately for different combinations of these variables. For left-handed incident electrons and τ^- (τ^+) emitted at forward (backward) polar angles, or for right-handed beam and τ^- (τ^+) in the backward (forward) region, the τ^- (τ^+) are predominantly left-handed (right-handed) and the pion energy spectrum is expected to be soft (Fig. 2(a)). For the two opposite combinations of P_e and $\cos\theta$, plotted in Fig. 2(b),the spectrum should be relatively hard since the decaying τ^- (τ^+) are predominantly right-handed (left-handed). Fig. 3 shows the same comparison for the $\tau \rightarrow \rho\nu_\tau$ decays. The difference is expected to be less obvious for the three-body decays $\tau \rightarrow \ell\bar{\nu}_\ell\nu_\tau$, but is still quite visible as shown in Fig. 4.

The tau neutrino helicity, h_{ν_τ}, and the Michel parameters ρ, ξ and $\xi\delta$ are determined using an unbinned maximum likelihood fit to the energy spectra of the decay channels $\tau \rightarrow \rho\nu_\tau$,$\tau \rightarrow \pi(\mathrm{K})\nu_\tau$ and $\tau \rightarrow \ell\bar{\nu}_\ell\nu_\tau$. The fit function is the theoretical differential cross section corrected for radiation and detector effects.

In the maximum likelihood technique, the following expression is minimized:

$$W = -2\ln\mathcal{L} = -2\sum_{n=1}^{N} \ln\left\{\frac{1}{\sigma}\frac{d^2\sigma}{d\cos\theta\, dz}\right\}_n , \qquad (12)$$

where $\mathcal{L}$ is the likelihood function. The sum in Eq. 12 runs separately over all τ's identified as either $\tau \rightarrow \mathrm{e}\bar{\nu}_e\nu_\tau$, $\tau \rightarrow \mu\bar{\nu}_\mu\nu_\tau$, $\tau \rightarrow \rho\nu_\tau$ or $\tau \rightarrow \pi(\mathrm{K})\nu_\tau$ candidates. The term in the logarithm is the differential cross-section for production of τ-pairs where one τ decays into one of these channels. This expression is corrected for effects of radiation, detector resolution, efficiency and backgrounds, and is normalized to unity.

The efficiencies and backgrounds were determined from Monte Carlo by studying the distribution of kinematic variables before and after event selection. The dependence of these functions on z and $\cos\theta$ is parameterized using low order polynomials. Details are given in Appendix II. The radiative correction functions are determined from the ratio of the spectrum generated using KORALZ [16] for events containing radiative effects to the spectrum of events generated with the Born level cross-sections. For details, see Appendix III. Since the spectra are different for decays of left- and right-handed taus, the correction functions are divided into four regions corresponding to combinations of positive or negative electron beam polarization and the forward or backward half of the detector. In each region either the left- or right-handed sample is enhanced.

Effects of detector resolution are studied using Monte Carlo for each input variable (e.g. track momentum or ω, and tau direction) in bins of that variable. From these studies the dependence of the mean and standard deviation are derived as a function of the value of the variable as generated by Monte Carlo, and these functions are used to correct the global resolution distributions. Finally, fits to multiple Gaussians are performed to model both the core and tails of the resolution distributions. Details are presented in Appendix III.

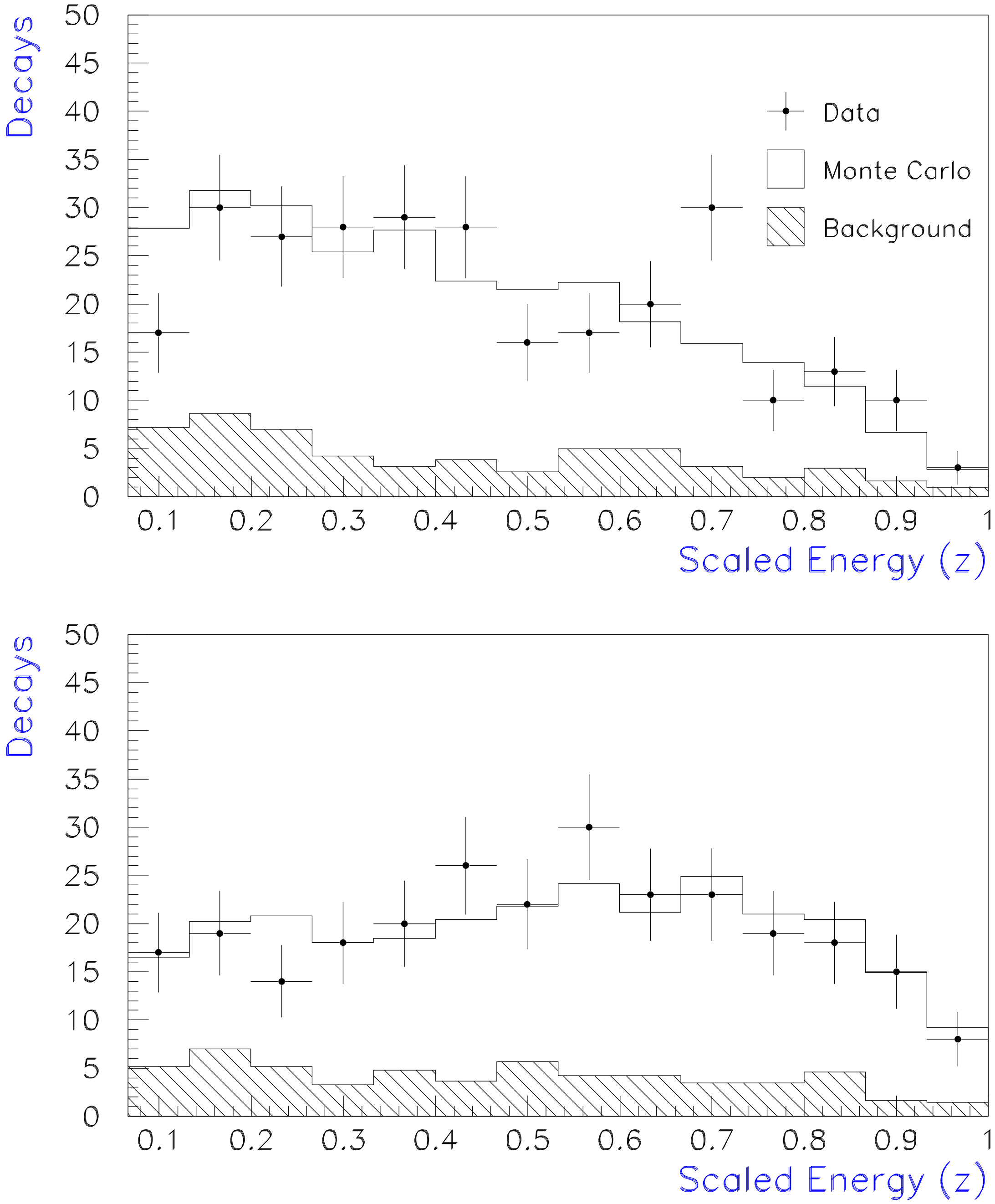

Figure 2: $\tau \rightarrow \pi(\mathrm{K})\nu_\tau$ decay energy spectra: (a) The sum of the spectra for pions in the forward direction with beam polarization $P_e < 0$ and in the backward direction with $P_e > 0$; (b) The sum of the spectra for pions in the backward direction with $P_e < 0$ and in the forward direction with $P_e > 0$. In each case the points are data and the histogram is from Monte Carlo.

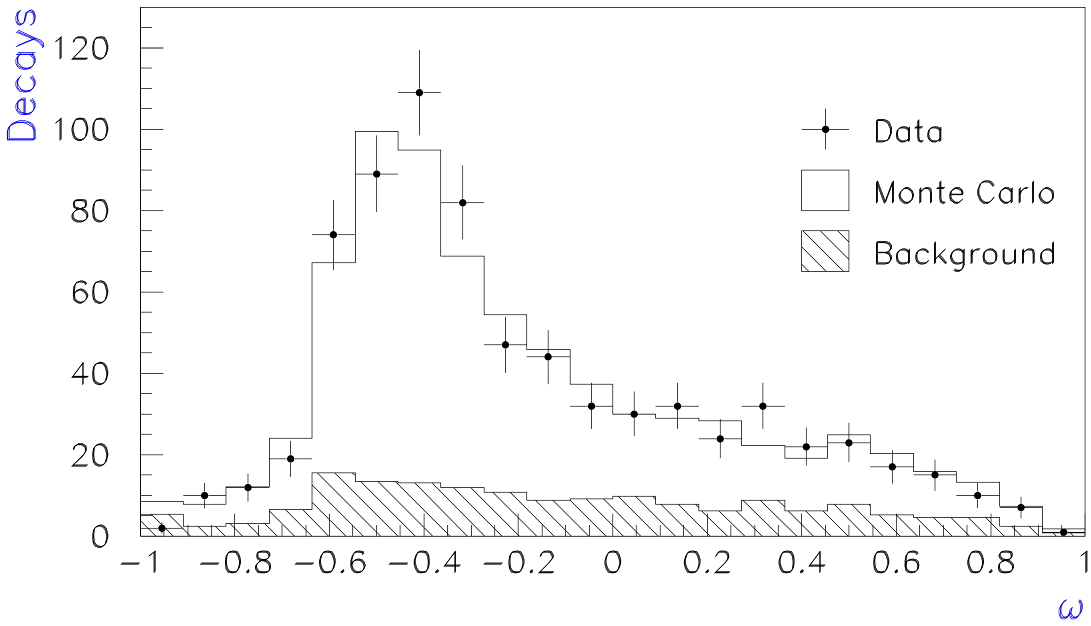

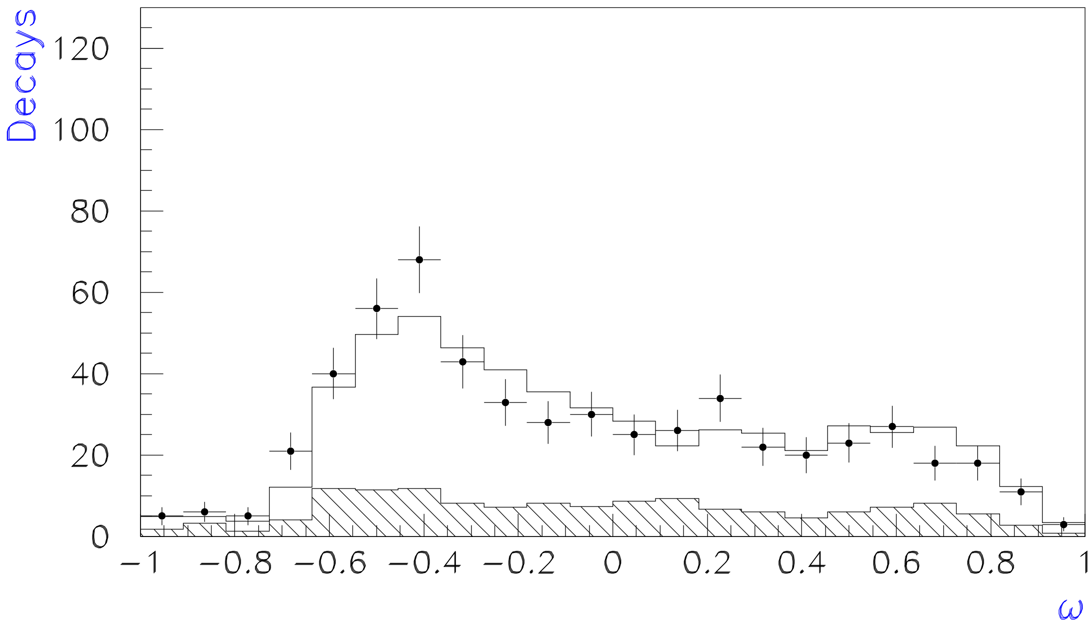

Figure 3: $\tau \to \rho\nu_\tau$ decay spectra: (a) The sum of the spectra for rhos in the forward direction with beam polarization $P_e < 0$ and in the backward direction with $P_e > 0$; (b) The sum of the spectra for rhos in the backward direction with $P_e < 0$ and in the forward direction with $P_e > 0$. The spectra are plotted against the quantity ω as defined in Section 1. In each case the points are data and the histogram is from Monte Carlo.

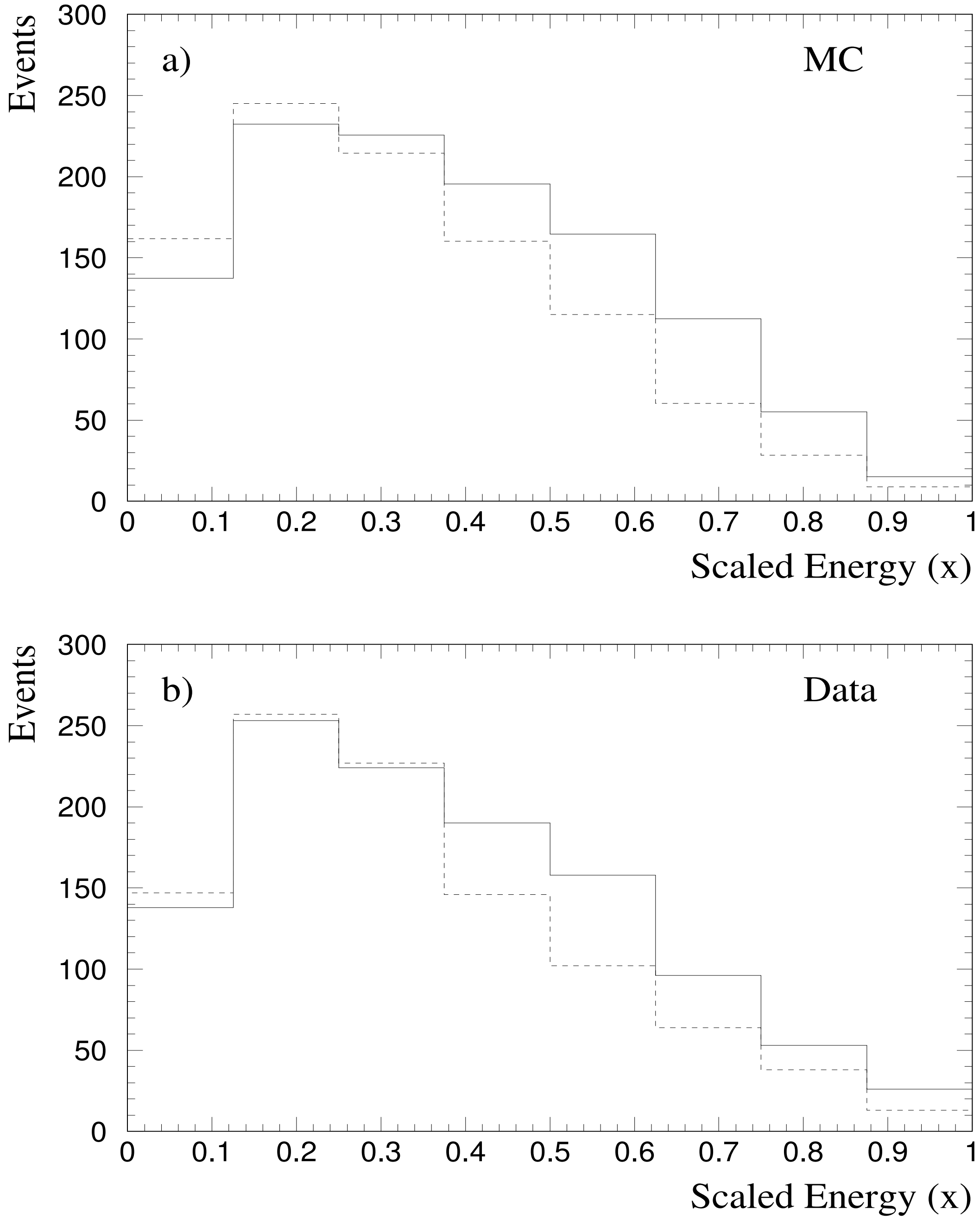

Figure 4: $\tau \rightarrow \ell \bar{\nu}_\ell \nu_\tau$ decay energy spectra from (a) Monte Carlo, and (b) the SLD data. For both histograms, the solid line is the sum of the spectra for leptons in the forward direction with beam polarization $P_e < 0$ and in the backward direction with $P_e > 0$, and the dashed line is the sum of the spectra for leptons in the backward direction with $P_e < 0$ and in the forward direction with $P_e > 0$.

5 Results and Discussion

Fitting the $\tau\to\pi(\mathrm{K})\nu_\tau$ and $\tau\to\rho\nu_\tau$ samples yields a combined result of $\mathrm{h}_{\nu_\tau} = -0.97 \pm 0.10(stat)$, which can be interpreted as the helicity of the tau neutrino. The fit to the $\tau\to\ell\bar{\nu}_\ell\nu_\tau$ channels gives $\xi = 1.03 \pm 0.36(stat)$, $\xi\delta = 0.84 \pm 0.27(stat)$, and $\rho = 0.71 \pm 0.09$.

The sources of systematic error which have been considered in the analysis include τ-pair selection efficiency and background, decay identification efficiency and background, resolution in z and $\cos\theta$, uncertainties in the measurements of the beam energy and polarization, and uncertainty in the value of A_ℓ [21]. Table 5 summarizes the systematic errors in our analysis. To investigate these errors, each parameter used in the fitting program is modified in turn by its uncertainty, and the fit is redone to obtain new values of h_{ν_τ}, ρ, ξ and $\xi\delta$. Any correlation between these input parameters is taken into account when combining the errors. Each error listed in Table 5 is a combination of several related contributions, and for the listed errors we assume they are not correlated. They are combined in quadrature to give the overall systematic error listed in the last row of the table.

	Δh_ν	$\Delta\rho$	$\Delta\xi$	$\Delta(\xi\delta)$
Final-state selection	0.021	0.008	0.032	0.015
Background	0.011	0.030	0.029	0.034
Radiative corrections	0.005	0.012	0.004	0.005
Resolution	0.027	0.026	0.020	0.024
Beam polarization	0.006	0	0.008	0.005
η	0	0.014	0.017	0.008
A_e, A_τ	0.008	0.004	0.004	0.008
TOTAL	0.038	0.045	0.052	0.046

Table 5: Systematic uncertainties.

A large contribution to the systematic uncertainty on ξ is the radiative correction, which affects the electron channel more strongly. The uncertainty in h_{ν_τ} is dominated by the π selection efficiency and the interference with the decay channels $\pi^\pm\mathrm{N}\pi^0$ (ρ, a_1, etc...).

Including systematic errors, the SLD values, by decay channel, for h_{ν_τ} are:

$$\begin{aligned}\mathrm{h}_{\nu_\tau}{}^{\pi} &= -0.86 \pm 0.18(stat) \pm 0.03(syst)\\ \mathrm{h}_{\nu_\tau}{}^{\rho} &= -1.03 \pm 0.12(stat) \pm 0.04(syst)\end{aligned}$$

results in a combined value of:

$$\mathrm{h}_{\nu_\tau} = -0.97 \pm 0.10(stat) \pm 0.04(syst)$$

and the Michel parameters ρ, ξ and $\xi\delta$ are:

$$\rho^e = 0.68 \pm 0.14(stat) \pm 0.06(syst)$$

$$
\begin{aligned}
\xi^e &= 1.18 \pm 0.52(stat) \pm 0.04(syst) \\
\xi\delta^e &= 0.79 \pm 0.44(stat) \pm 0.07(syst) \\
\\
\rho^\mu &= 0.74 \pm 0.13(stat) \pm 0.06(syst) \\
\xi^\mu &= 0.89 \pm 0.49(stat) \pm 0.08(syst) \\
\xi\delta^\mu &= 0.87 \pm 0.35(stat) \pm 0.05(syst)
\end{aligned}
$$

where the combined values are:

$$
\begin{aligned}
\rho &= 0.71 \pm 0.09(stat) \pm 0.05(syst) \\
\xi &= 1.03 \pm 0.36(stat) \pm 0.05(syst) \\
\xi\delta &= 0.84 \pm 0.27(stat) \pm 0.05(syst).
\end{aligned}
$$

The matrix element of a τ leptonic decay can be written as a four fermion interaction in the following way

$$
\mathcal{M} = \frac{4G_F}{\sqrt{2}} \sum_{\gamma,\epsilon,\mu,n,m} g^\gamma_{\epsilon\mu} \langle \bar{\ell}_\epsilon | \Gamma^\gamma | \nu_\ell{}^n \rangle \langle \bar{\nu}^m_T | \Gamma_\gamma | \tau_\mu \rangle, \tag{13}
$$

where the index γ labels the different types of interactions: scalar, vector or tensor, ϵ and μ stand for the chiral projection of the ℓ and τ lepton spinors , n and m represent the handness of the $\bar{\nu}_\ell$ and the ν_T. The leptonic charged weak interaction for e and μ were already measured precise enough to exclude interactions different from a pure $(V-A)$ at the $\ell\bar{\nu}_\ell$ vertex [22]. Therefore, one can assume a $(V-A)$ at the $\ell\bar{\nu}_\ell$ vertex and allow a combination of $(V-A)$ and $(V+A)$ at the τ one [23]. This assumption reduces the number of parameters that determine the characteristic of the $\tau\nu_\tau$ to one free parameter as in the hadronic decay channels. With that the relation between h_{ν_τ} and ρ, ξ, δ are the following [24]:

$$
\mathrm{h}_{\nu_\tau} = 1 - \frac{8}{3}\rho = \xi - 2 = 1 - \frac{8}{3}\xi\delta \tag{14}
$$

Hence using these relation we can interpret the leptonic decay channels results as $\mathrm{h}_{\nu_\tau}{}^{leptons} = -0.95 \pm 0.21$, and combined with the hadronic decay channels one gets $\mathrm{h}_{\nu_\tau}{}^{lept+had} = -0.97 \pm 0.09$ which can be also interpreted as $\frac{2g_V^W g_A^W}{(g_V^W)^2+(g_A^W)^2}$.

The results are consistent with the Standard Model V-A predictions of -1, $\frac{3}{4}$, 1, $\frac{3}{4}$. These measurements provide an interesting cross check with other experimental results ([25] - [28]) since this analysis does not rely on spin correlations is the first measurement to be performed with polarized beams and unlike the correlation methods it provides the sign of ξ and h_{ν_τ} as well as their magnitude. These results demonstrate the power of polarized beams for probing deviations from the Standard Model in the weak couplings.

References

[1] Y.S. Tsai, *Phys. Rev.* **D4** (1971) 2821.

[2] Morris Swartz *SLD Physics Note* **21** (1992).

[3] J.E. Brau and G.J. Tarnopolsky *Phys. Rev.* **D24** (1981) 2541.

[4] A Rougé *Z. Phys.* **C48** (1990) 75.

[5] M. Davier *et al., Phys. Lett.* **B306** (1993) 411.

[6] L. Michel, *Proc. Phys. Soc.* **A63** (1950) 514.
C. Bouchiat and L. Michel, *Phys Rev.* **106** (1957) 170.

[7] K. Mursula, M. Roos, F. Scheck, *Nucl. Phys.* **B219** (1989) 321.
W. Fetscher H.J. Gerber, K.F. Johnson, *Phys Lett.* **B173** (1986) 102.

[8] M. Daoudi, Proceedings of the International Europhysics Conference on High Energy Physics, Brussels, Belgium, 1995, edited by J. Lemonne, C. Vander Velde, and F. Verbeure (World Scientific Publ., Singapore, (1995) 625;
K. Abe *et al.,* "Measurement of the τ Charged Weak Couplings with SLC Polarized Beams," SLAC-PUB-95-6971, contributed to the 1995 International Symposium on Lepton and Photon Interactions at High Energies, Beijing, China.
A. McKemey "Tau Lorentz Structure with Polarization at SLD", proceedings of the XXVIII International Conference on High Energy Physics, July/96, Warsaw, Poland.

[9] SLD Design Report, *SLAC-REPORT-273*, May 1984.

[10] M. Fero *et al., Nucl. Instr. Methods* **A367** (1995) 111.

[11] C.J.S. Damerell *et al.,* "Design and Performance of the SLD Vertex Detector, a 120 MPixel Tracking System", Proceedings of the 26th Int. Conf. on High Energy Physics, Dallas, Texas, August 1992;
M. Strauss *et al.,* "Performance of the SLD CCD Pixel Vertex Detector and Design of an Upgrade," Proceedings of the 27th Int. Conf. on High Energy Physics, Glasgow, Scotland, July 1994.

[12] D. Axen *et al., Nucl. Instr. Methods* **A328** (1993) 472.

[13] K. Abe *et al., Nucl. Instr. Methods* **A343** (1994) 74.

[14] A. C. Benvenuti *et al., Nucl. Instr. Methods* **A290** (1990) 353.

[15] SLD Collaboration, K. Abe *et al., Phys. Rev.* **D52** (1995) 4828.

[16] S. Jadach, B.F.L Ward and Z. Was, *Comp. Phys. Comm.* **79** (1994) 503.

[17] H. Anlauf *et al., Comp. Phys. Comm.* **79** (1994) 466.

[18] H. Aihara *et al., Phys. Rev. Lett.* **58** (1987) 97; and references therein.

[19] T. Sjöstrand,*Comp. Phys. Comm.* **82** (1994) 74.

[20] GEANT program, version 3.21, CERN Application Software Group, *CERN Program Library* (1994).

[21] The SLD asymmetry value $A_\ell = 0.1543 \pm 0.0039$ is used. See SLAC-PUB-7234, E. Torrence, Proceedings of the XXVIII International Conference on High Energy Physics, Warsaw, Poland, July 1996.

[22] W. Fetscher, H.J. Gerber, and K.F. Johnson, *Phys Lett.* **B173** (1986) 102.
R.M. Barnett *et al., Phys. Rev.* **D54** (1996) 201.

[23] P. Privitera, Phys. Lett. **B288** (1992) 227.

[24] Erez Etzion, "Analysis of the Tau Polarization and its Forward-Backward Asymmetry on the Z0", *hep-ex/9606011*, PhD Thesis, Tel-Aviv University, (1994) 143.

[25] ARGUS collaboration, H. Albrecht *et al., Phys. Lett.* **B337** (1994) 383;
Phys. Lett. **B349** (1995) 576.

[26] ALEPH Collaboration, D. Buskulic *et al., Phys. Lett.* **B346** (1995) 379.

[27] CLEO Collaboration, J. Bartelt *et al.,* "$\pi^-\pi^+$ Energy Correlation in τ Pair Events", Proceedings of the 27th Int. Conf. on High Energy Physics, Glasgow, Scotland, July 1994.

[28] L3 Collaboration, M. Acciarri *et al., Phys. Lett.* **B377** (1996) 313.

6 Appendix I - Event Selection

The selection of tau-pair candidates is based on the multiplicity, momentum and direction of tracks in the SLD central drift chamber, and on properties of electromagnetic clusters in the calorimeter. Tracks and energy clusters are required to meet certain criteria to be used in this selection.

6.1 Track and cluster requirements

Drift chamber tracks are required to satisfy the following: There must be at least 20 hits on each track, each track must project within 6 cm of the interaction point along the beam line and within 3 cm transverse to the beam line, the transverse momentum of the track must be greater than 100 MeV/c, the track fit $\sqrt{\chi^2} - \sqrt{2ndf} < 10$, and any pairs of oppositely charged tracks which are consistent with originating from a photon conversion are rejected.

In the calorimeter, any energy deposition consistent with originating from background muons moving parallel to the SLC beam is discarded. Energy clusters are then required to satisfy the following: A cluster must have at least 10 MeV in the first layer of the EM section and at least 20 MeV in the second EM layer, the total cluster energy must be at least 100 MeV.

6.2 Definition of event quantities

The visible energy, missing momentum and jet masses in each event are calculated using charged tracks in the drift chamber and neutral clusters in the calorimeter. Neutral clusters are defined as those which have no track projecting within 3 mrad of any tower included in the cluster. The energy of a neutral cluster and the position of the energy-weighted centroid are used to calculate a momentum vector associated with the cluster. The "missing momentum" vector is defined as the vector sum of all charged track and neutral cluster momenta, while the visible energy is defined as the scalar sum of the magnitudes. The jet axis in each hemisphere is defined by the direction of the vector sum of momenta of tracks in the hemisphere. Neutral clusters with 15° of these jet axes are included in the jets.

6.3 Selection of candidates

Tau-pair candidates are required to have fewer than seven tracks and at least one track in each hemisphere. Each event is divided into hemispheres by the plane normal to the track with the highest momentum. Tracks in each hemisphere must fall within 15° of the net momentum in the hemisphere, and the jet invariant mass in each hemisphere is required to be less than 2.3 GeV/c^2. Furthermore, the jet axes in the two hemispheres must be back-to-back within 20°. These criteria discriminate strongly against background from multihadron final states. The polar angle Θ_{miss} of the missing momentum in each event is required to satisfy $|cos\Theta_{miss}| < 0.88$ to discriminate against two-photon interactions and Bhabha events. Two-prong events are required to have a minimum acolinearity of 10 mrad. The scalar sum of the momenta of the two stiffest tracks in any event must be less than 65 GeV/c. These cuts primarily reject Bhabha events and muon-pair final states.

The total visible energy in an event is required to be at least $10GeV$ to reject two-photon interactions. To discriminate against Bhabha events, the total energy deposited in the EM section of the calorimeter is required to be less than 62.5 GeV. In addition, the total calorimeter energy not included in identified jets is required to be less than 5 GeV, and there must be fewer than nine energy clusters not included in jets.

The resulting efficiency is $62.7 \pm 0.1\%$. The background fractions determined from Monte Carlo are given in Table 6.

Background	Percentage of Sample %
Bhabha	0.84 ± 0.11
μ-pairs	0.94 ± 0.09
Multi-hadrons	0.28 ± 0.08
2γ	0.53 ± 0.07
Total	2.59 ± 0.18

Table 6: Background composition to selected τ events.

6.4 $\tau \rightarrow \rho\nu_\tau$ Event Selection

Selected tau events are divided into hemispheres by the plane normal to the events thrust axis, and the hemispheres are treated independently. Any pairs of oppositely charged tracks which are consistent with originating from a photon conversion are removed, and the hemispheres are then required to have only one track. Electron and muons are rejected by a series of hybrid cuts applied with increasing strength, making use of the electromagnetic and muon calorimeter information. To prevent correlated π and ρ data samples, the $\tau \rightarrow \pi\nu$ selection, as described in section 3, is used to reject events.

The remaining tau events are then categorized according to the number of calorimeter clusters found within a 20^0 cone of the thrust axis, after eliminating clusters from SLC muons.

Category 1 events are those with 1 cluster. Since both tracks with matched and unmatched clusters are considered it is necessary to divide this sample.

Category 1 candidates with an associated cluster must have greater than 2 hit towers in layer one of the electromagnetic section of the calorimeter, $KHIT1$, except for $cos\theta_{thrust} \geq 0.6$ in which case $KHIT1 \geq 6$. In addition, the opening angle between the track and the cluster must be greater than 19mrad and the unscaled energy of the cluster, E, divided by the the momentum of the track, p, must be greater than 0.53 for $p > 15GeV$, otherwise this quantity must be greater than $(0.53 + ((p-15)/16)^2)$.

Category 1 candidates with an unassociated cluster must have, $2 \leq KHIT1 \leq 10$ for $cos\theta_{thrust} \geq 0.6$, otherwise $3 \leq KHIT1 \leq 16$, and $E/p \geq 0.2$.

Category 1 candidates are then further subdivided into clusters containing minimum ionizing tracks and clusters containing significant hadronic energy. The clusters containing minimum ionizing tracks must satisfy the following criteria, the unscaled energy in layer two of the EM section is required to be, $E_{EM2} > 0.5$ GeV and the energy in layer one of the hadronic section must be $E_{Had1} > 0.5$ GeV. The rho energy, E_ρ, and mass, m_ρ, is then calculated using the cluster's average $cos\theta$ and ϕ, the total energy of the cluster on the EM scale and the momentum of the track.

For the remaining candidates from category 1, the energy of the track, calculated from the momentum of the track assuming it is a pion, is subtracted from the hadronic scaled energy of the cluster, the remaining energy is then scaled according to the EM scale. The rho energy and mass is then calculated using this energy, the cluster's average $cos\theta$ and ϕ in the EM section of the calorimeter and the track momentum.

Category 2 events have two clusters. The cluster which is associated with the track is assumed to have originated from a pion and the remaining cluster is assumed to be two photons from the π^0. For the unassociated cluster, the ratio of the energy is layer one of the electromagnetic calorimeter divided by the total energy in the LAC is required in the range, $0.18 \leq E_{EM1}/E_{Tot} \leq 0.96$. The associated cluster must have a value of $E/p \leq 0.56$.

The rho energy and mass is calculated using the track momentum, average unassociated cluster $cos\theta$ and ϕ and total unassociated cluster energy, scaled according to the EM scale. The rejected sample is then reconsidered under the criteria of category 1, the associated cluster being the cluster which is considered.

Category 3 events have three clusters. One of the clusters must be associated with the track and the remaining two are assumed to be photons from the π^0. The unassociated clusters are roughly filtered by requiring them to have a value of $E_{EM1}/E_{Tot} \leq 0.96$. If both unassociated clusters fail this criteria, the event is reassessed using category 1.

A π^0 mass, m_{π^0}, is formed using the EM scaled cluster energies and average cluster $cos\theta$ and ϕ (see Fig. 5). The rho energy and mass is calculated for candidates which have, $0.09 \leq m_{\pi^0} \leq 0.21$, using the track momentum and calculated energy. Finally, the total energy of the clusters divided by the rho energy, $E/E_\rho \leq 0.98$.

The last category, Category 4 have greater than three clusters, one of which must be associated with the track. Under category 2 and 3, an attempt is made to reconstruct values of E_ρ and m_ρ. For category 2, if more than one track-cluster combination is found to lie within the rho mass window it is rejected. For category 3, if more than one π^0 candidate is found then the event is rejected. Events reaching the final sample will be classified as either category 2 or 3, if the event passes both criteria, category 2 takes precedent.

Finally all rho candidates are required to lie within a rho mass window, $0.44 \leq m_\rho \leq$

1.2, figure 6.

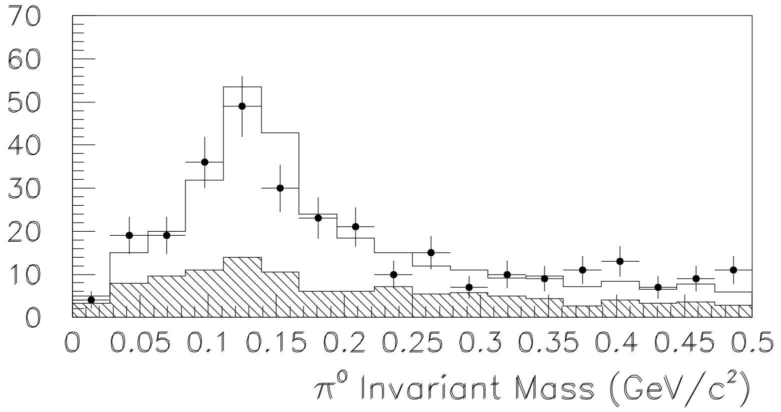

Figure 5: Data/MC comparison of the reconstructed π^0 invariant mass for Category 3 ρ candidates. The unshaded histogram is all selected MC events, the shaded histogram is selected MC background events and the points are the data.

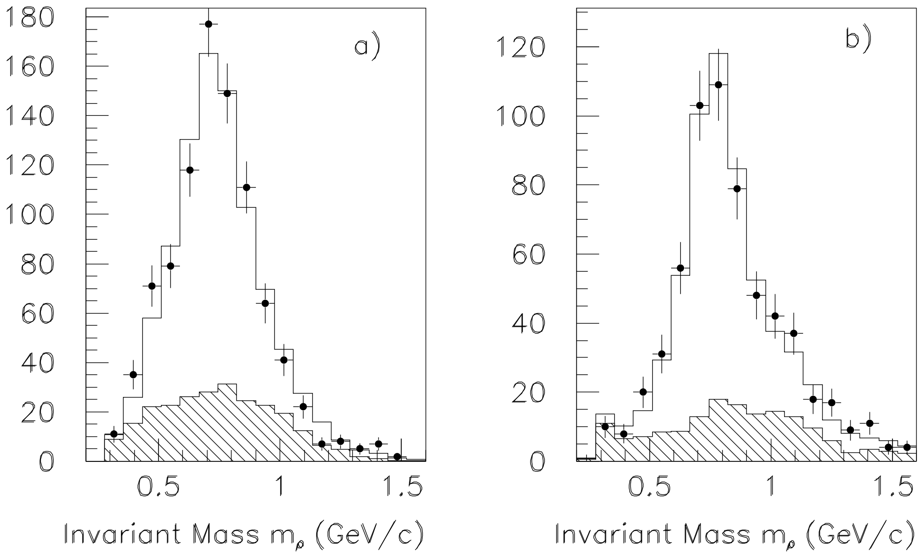

Figure 6: Data/MC comparison of the reconstructed ρ invariant mass. The unshaded histogram is all selected MC events, the shaded histogram is selected MC background events and the points are the data. Figure a) shows Category 1 candidates and figure b) shows category 2,3 and 4 candidates combined.

7 Appendix II - Efficiency and Background parameterization

The selection efficiency and background were studied using fully reconstructed Monte Carlo. The tau selection efficiency and tau decay selection efficiency were studied separately, as a function of the generated $|cos\theta_\tau|$ and ω. Low order polynomials were used to characterize the distributions, the resulting function being used to correct the theoretical functions prior to convolution with the resolution functions. The corrections were studied separately for the left hand and right hand enhanced samples and a combined parameterization was used only when the parameterization of both were in good agreement.

Since the background parameterization is applied after the theoretical function has been convoluted with resolution function, it was studied as function of the reconstructed $|cos\theta_{thrust}|$ and ω. Again, low order polynomials were used to characterize the background distributions. However, this time binning was selected to maintain a less than 10 % error on each parameter of the best fit.

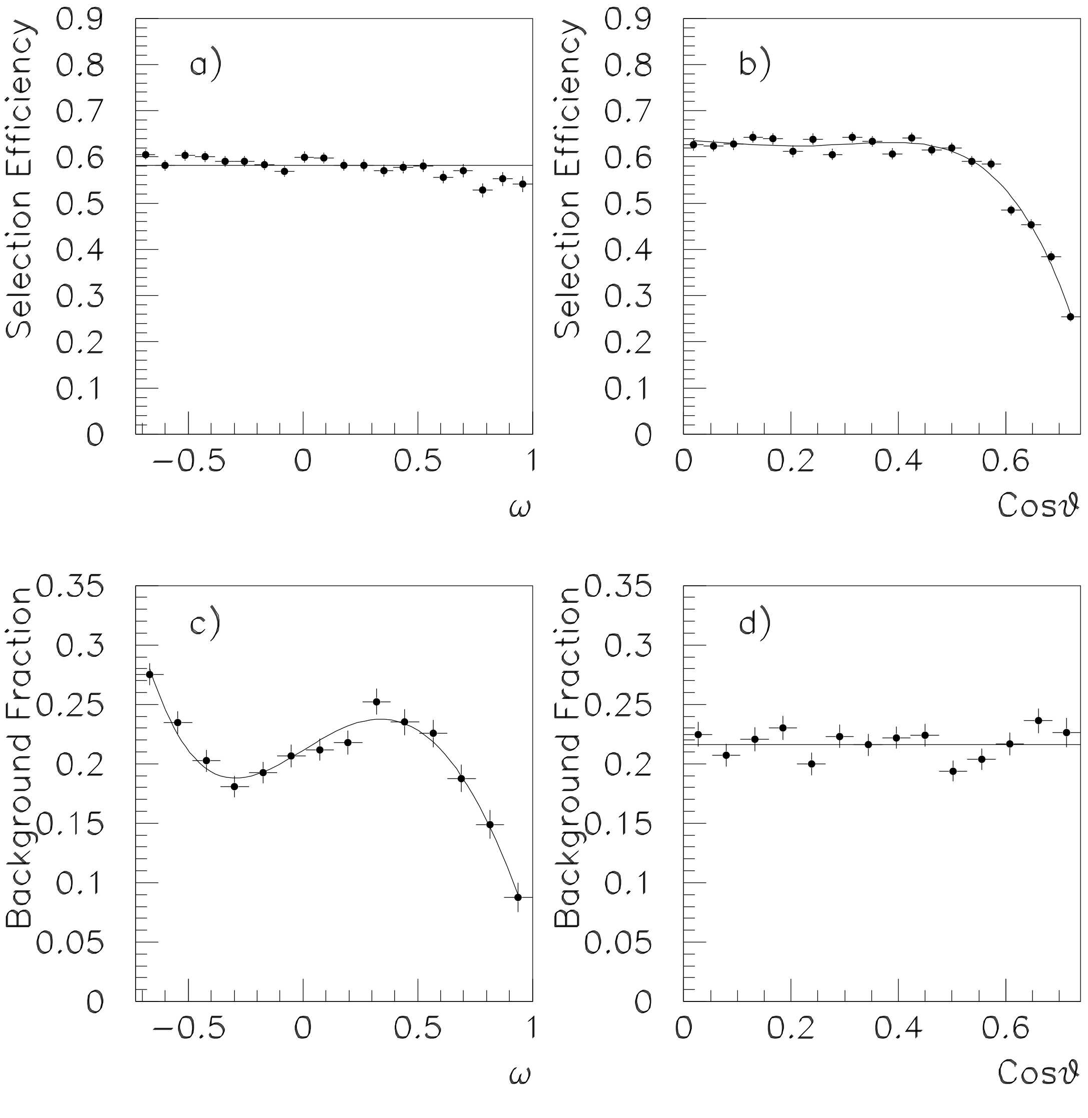

Figure 7: $\tau \rightarrow \pi(\mathrm{K})\nu_\tau$ selection efficiency (a,b) and background (c,d) as a function of ω and $\cos\theta$.

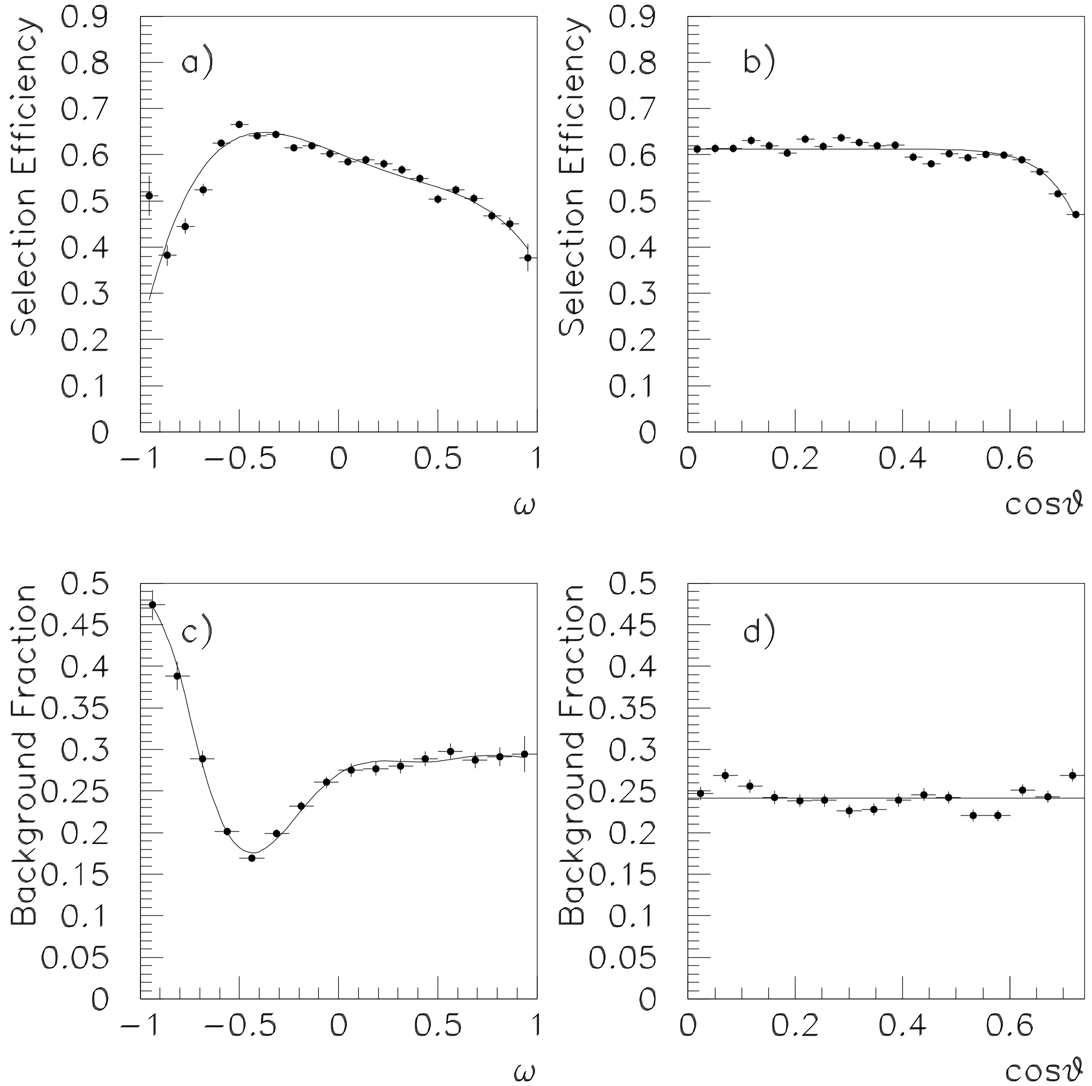

Figure 8: $\tau \to \rho\nu_\tau$ selection efficiency (a,b) and background (c,d) as a function of ω and $\cos\theta$.

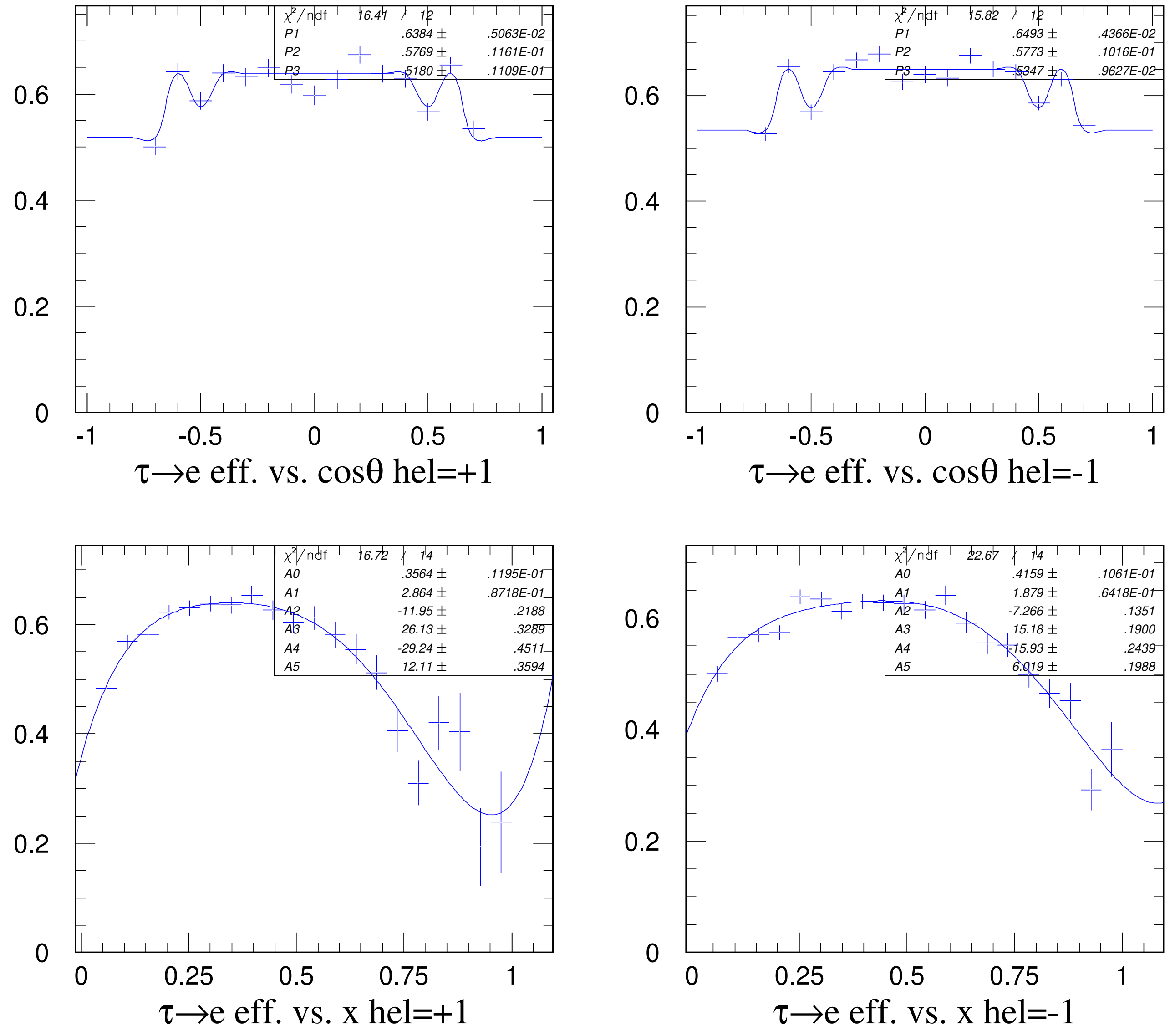

.

Figure 9: The Monte Carlo estimated efficiency versus $\cos\theta$ (a,b) and scaled energy (c,d) for tau decays to electrons. Plots (a,c) for right hand enhanced taus and (b,c) for left handed enhanced taus.

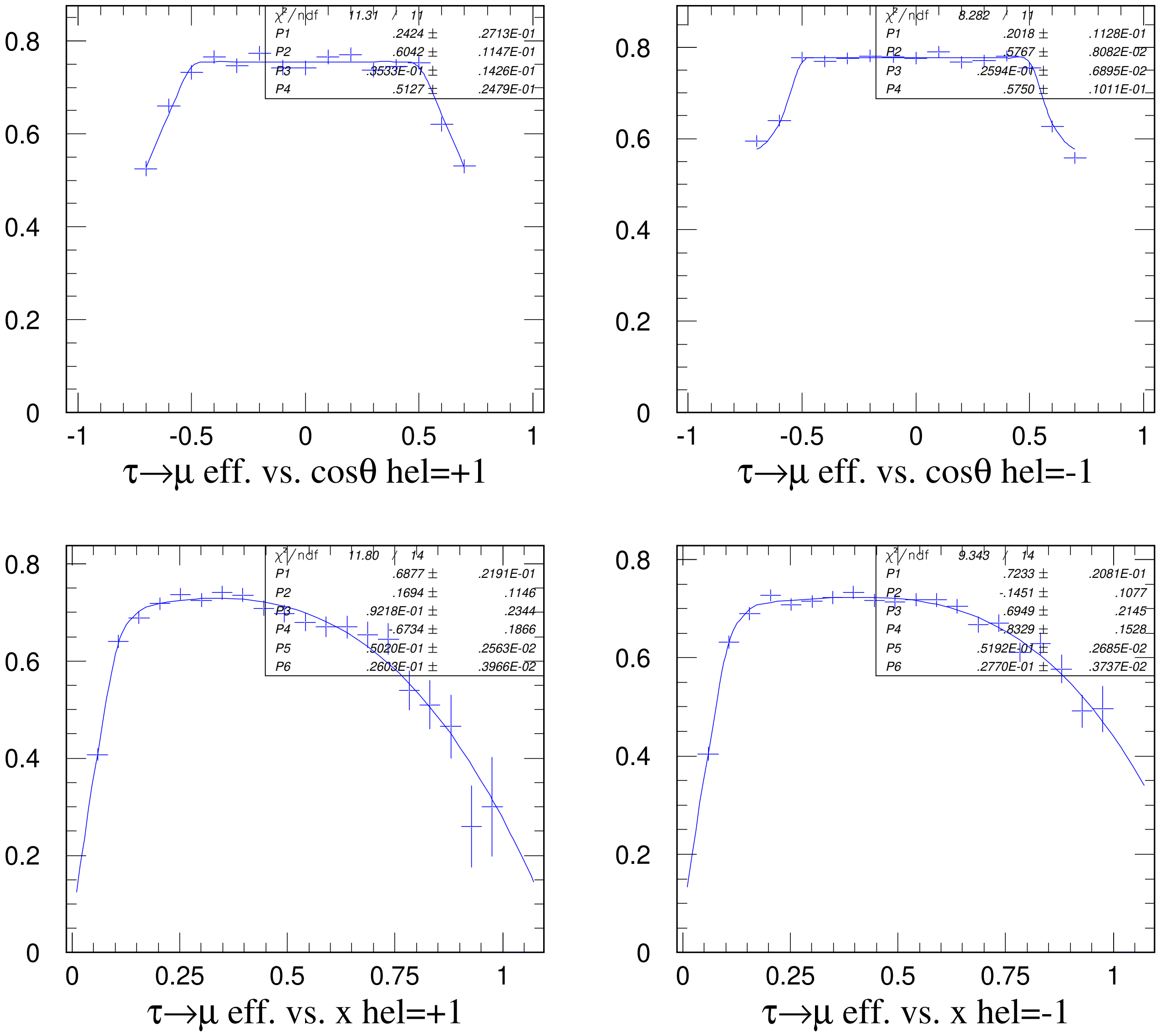

.

Figure 10: The Monte Carlo estimated efficiency versus $\cos\theta$ (a,b) and scaled energy (c,d) for tau decays to muons. Plots (a,c) for right hand enhanced taus and (b,c) for left handed enhanced taus.

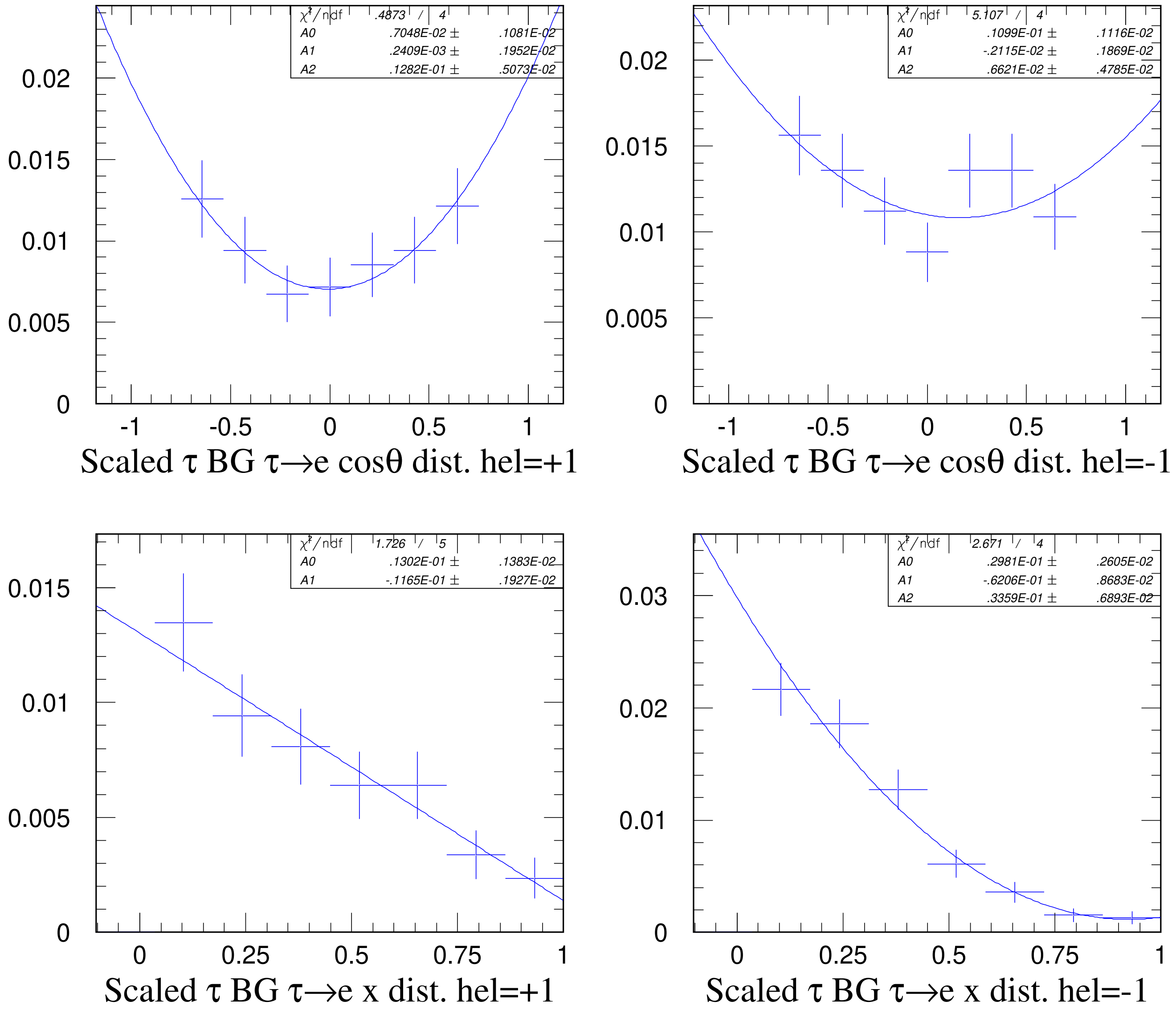

.

Figure 11: The Monte Carlo estimated tau background fraction versus $\cos\theta$ (a,b) and scaled energy (c,d) for tau decays to electrons. Plots (a,c) for right hand enhanced taus and (b,c) for left handed enhanced taus.

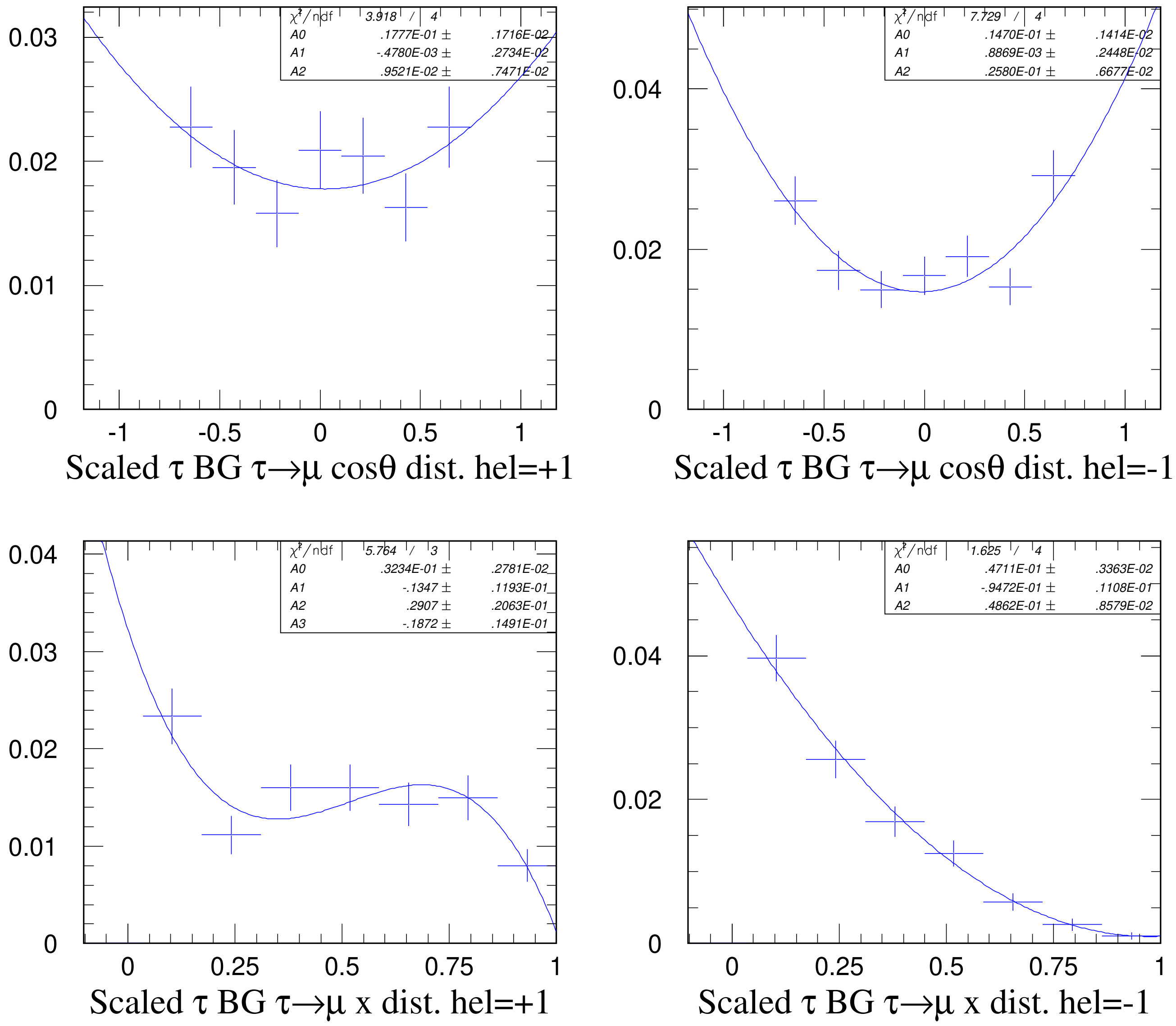

.

Figure 12: The Monte Carlo estimated tau background fraction versus $\cos\theta$ (a,b) and scaled energy (c,d) for tau decays to electrons. Plots (a,c) for right hand enhanced taus and (b,c) for left handed enhanced taus.

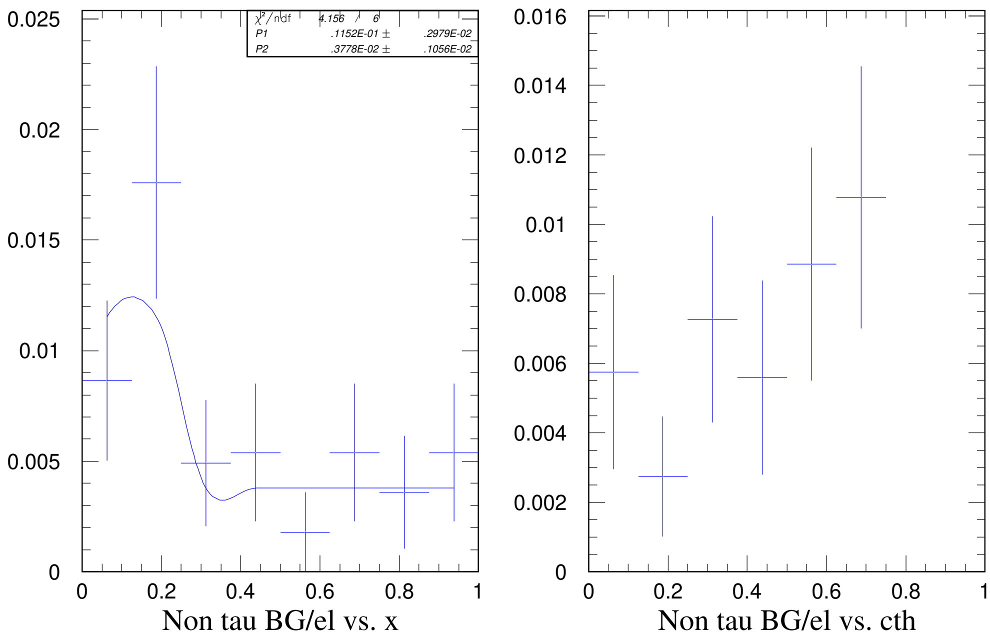

.

Figure 13: The Monte Carlo estimated non tau background fraction versus and scaled energy (a) and $\cos\theta$ (b) for tau decays to electrons.

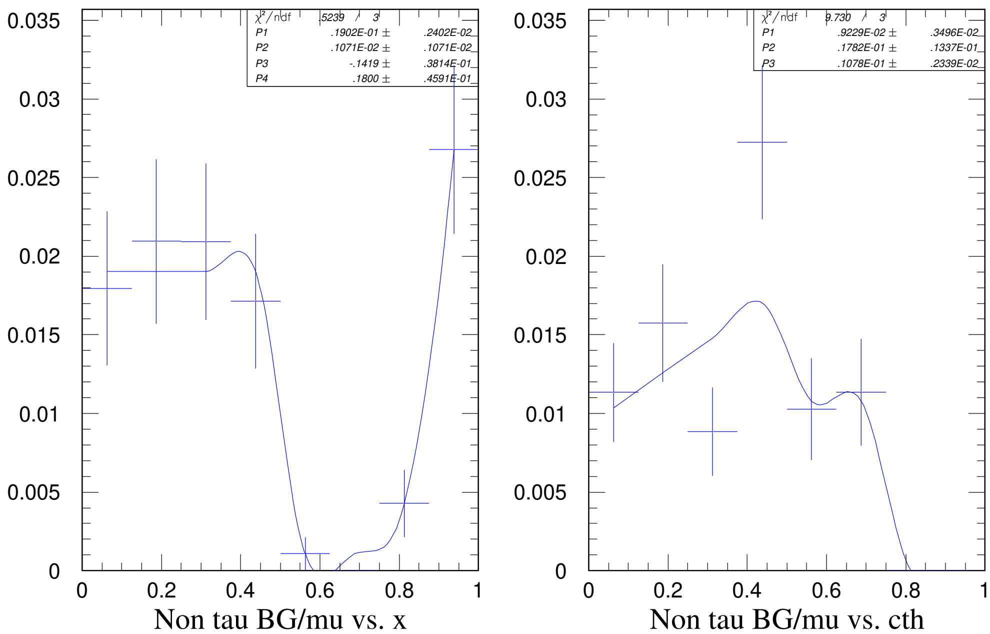

.

Figure 14: The Monte Carlo estimated non tau background fraction versus and scaled energy (a) and $\cos\theta$ (b) for tau decays to muons.

8 Appendix III - Resolution and Radiative Correction Studies

8.1 Pi and Rho Resolution

The resolution functions are derived in a similar fashion for both ω and $cos\theta$. The underlying assumption is that the Monte Carlo is a true representation of the data. This can only be tested by comparing data and Monte Carlo.

The first step is to investigate for variations of the sigma σ and mean μ of the variable deviation as a function of the MC generated value. This is done by plotting the generated value of the variable, X_{true}, minus the reconstructed value, X, in bins of X_{true} and fitting a Gaussian to the resulting distribution. This yields a $\sigma(X_{true})$ and $\mu(X_{true})$ function. This is then used to correct the distribution,

$$\mathcal{R}(X, X_{true}) = \frac{(X_{true} - X) - \mu(X_{true})}{\sigma(X_{true})} \tag{15}$$

A multiple Gaussian fit is used to parameterize the distribution. Subsequently, when fitting to the data, this is convoluted with the theoretical function effectively smearing the function to agree with that expected from data. The parameterization are shown in Figs. 15-19.

Cross checks are performed at this stage to determine whether the resolution function has other dependences. Hence, $cos\theta$ is investigated as a function of ω and both $cos\theta$ and ω have been studied separately for the left hand and right hand enhanced case. All of the above studies showed no significant dependence.

8.2 Electron and Muon Resolution

Momentum and $\cos\theta$ resolutions are studied using the fully reconstructed tau Monte Carlo set. Selected $\tau \to e\bar{\nu}_e\nu_\tau$ and $\tau \to \mu\bar{\nu}_\mu\nu_\tau$ events are binned by their true Monte Carlo momenta and δp ($p_{MC} - p_{measured}$) over p distributions are constructed. These distributions are fit using three Gaussians. For the muons, we determine a fixed shape from these fits and re-fit holding the relation between the three Gaussians constant while varying the overall width and mean of the distribution to determine the momentum dependence of the shape parameters. The shape is verified by comparison with the shape derived from selected mu pairs in the data. For the electrons, we find that the shape of the distribution is momentum dependent due to the use of the calorimeter in addition to the tracking to determine the electron momentum. As a result, we fit separately for the momentum dependence of the three Gaussians. We check for $\cos\theta$ dependencies by making $\delta p/p$ distributions for bins in $\cos\theta$. We find that any $\cos\theta$ dependency of the momentum resolution is negligible within our acceptance. The $\cos\theta$ resolution is determined using a similar procedure, where we find that like the muon momentum resolution, the shape is momentum and $\cos\theta$ independent and fit for the dependencies of the overall width and mean. The parameterization of the electrons and muons momentum resolution are shown in Figs. 20-21.

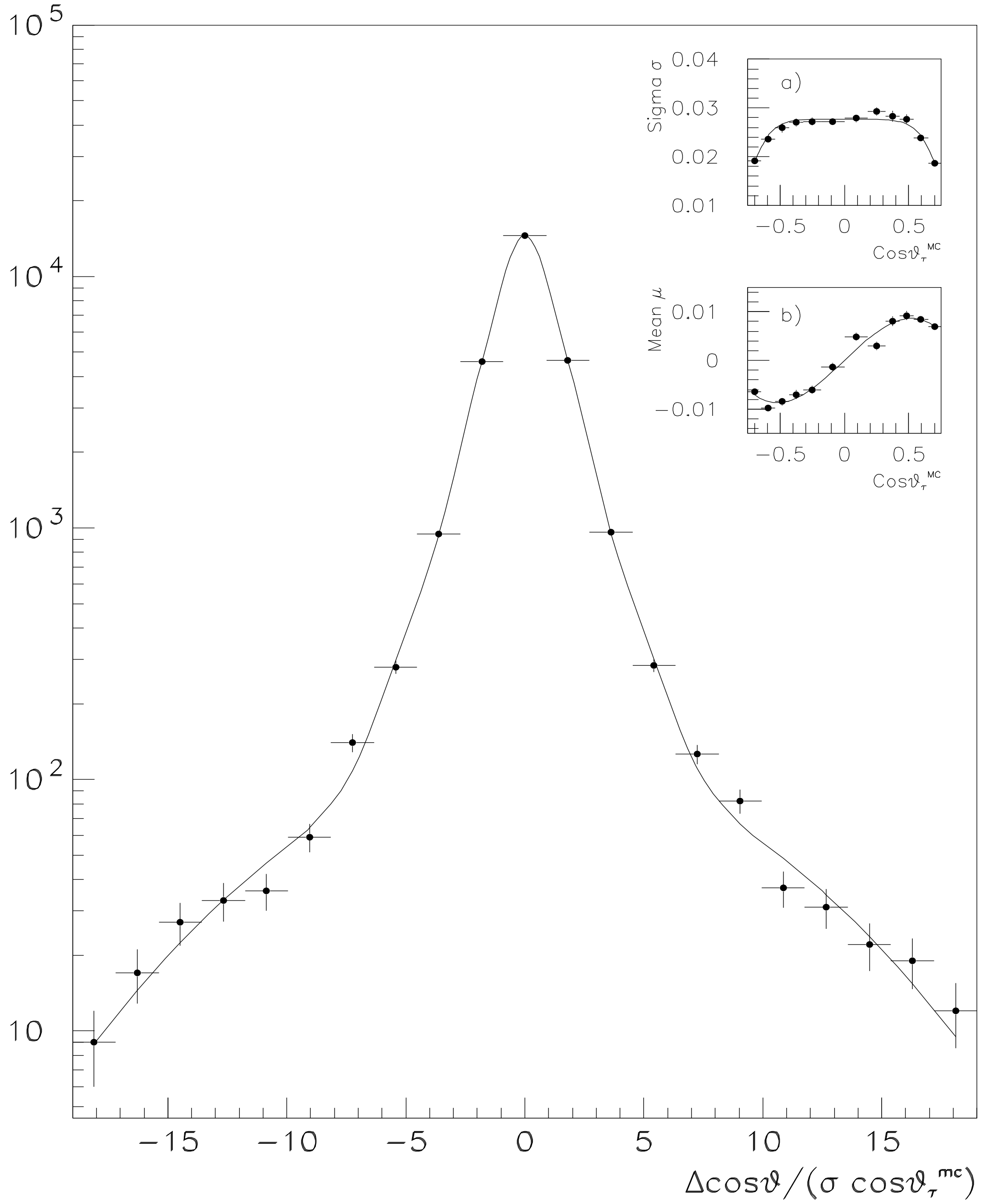

Figure 15: $\cos\theta$ Resolution for $\tau\to\pi(\mathrm{K})\nu_\tau$ events.

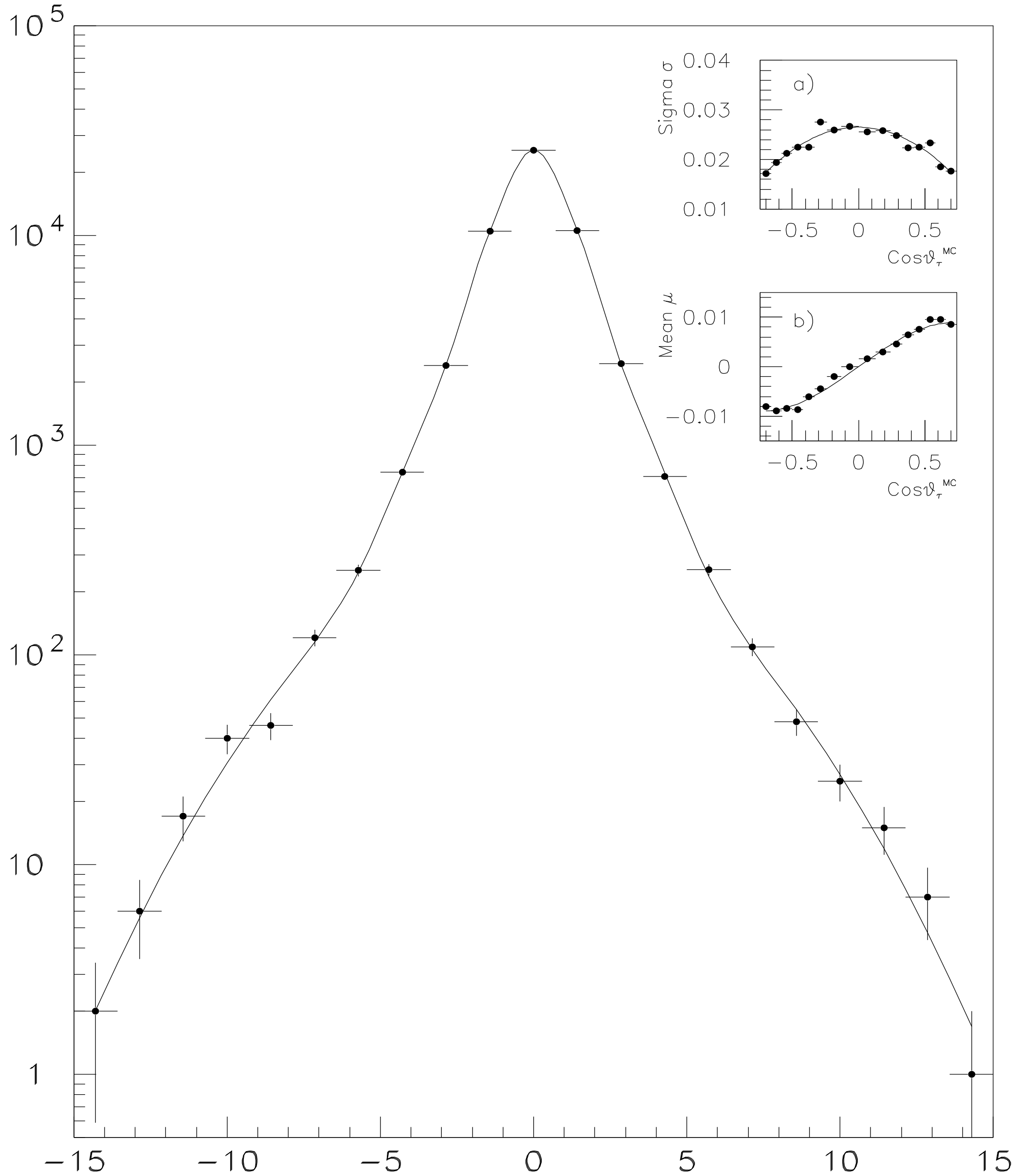

Figure 16: $\cos\theta$ Resolution for $\tau \rightarrow \rho\nu_\tau$ events.

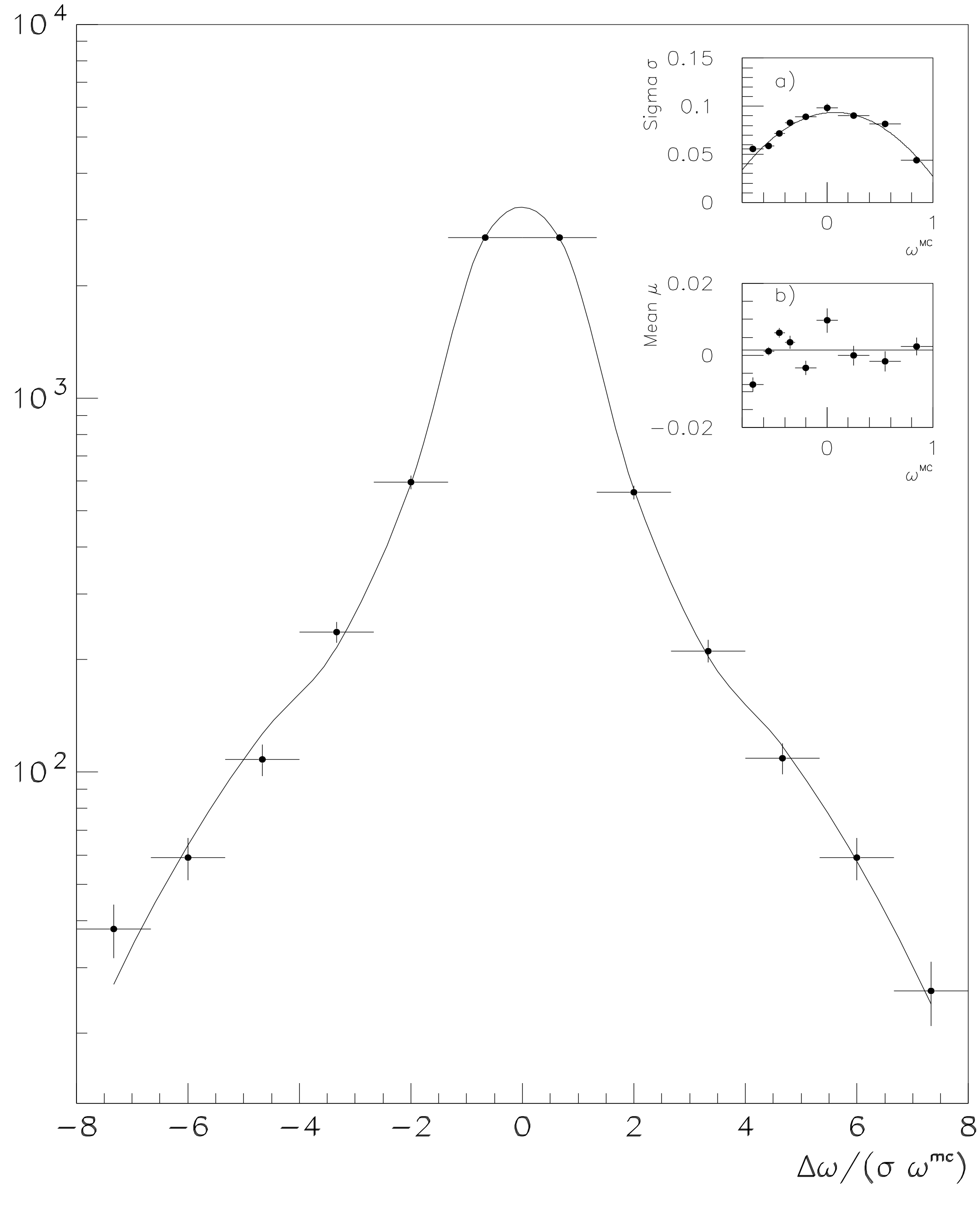

Figure 17: ω Resolution for "Left Hand enhanced" $\tau \to \rho\nu_\tau$ events.

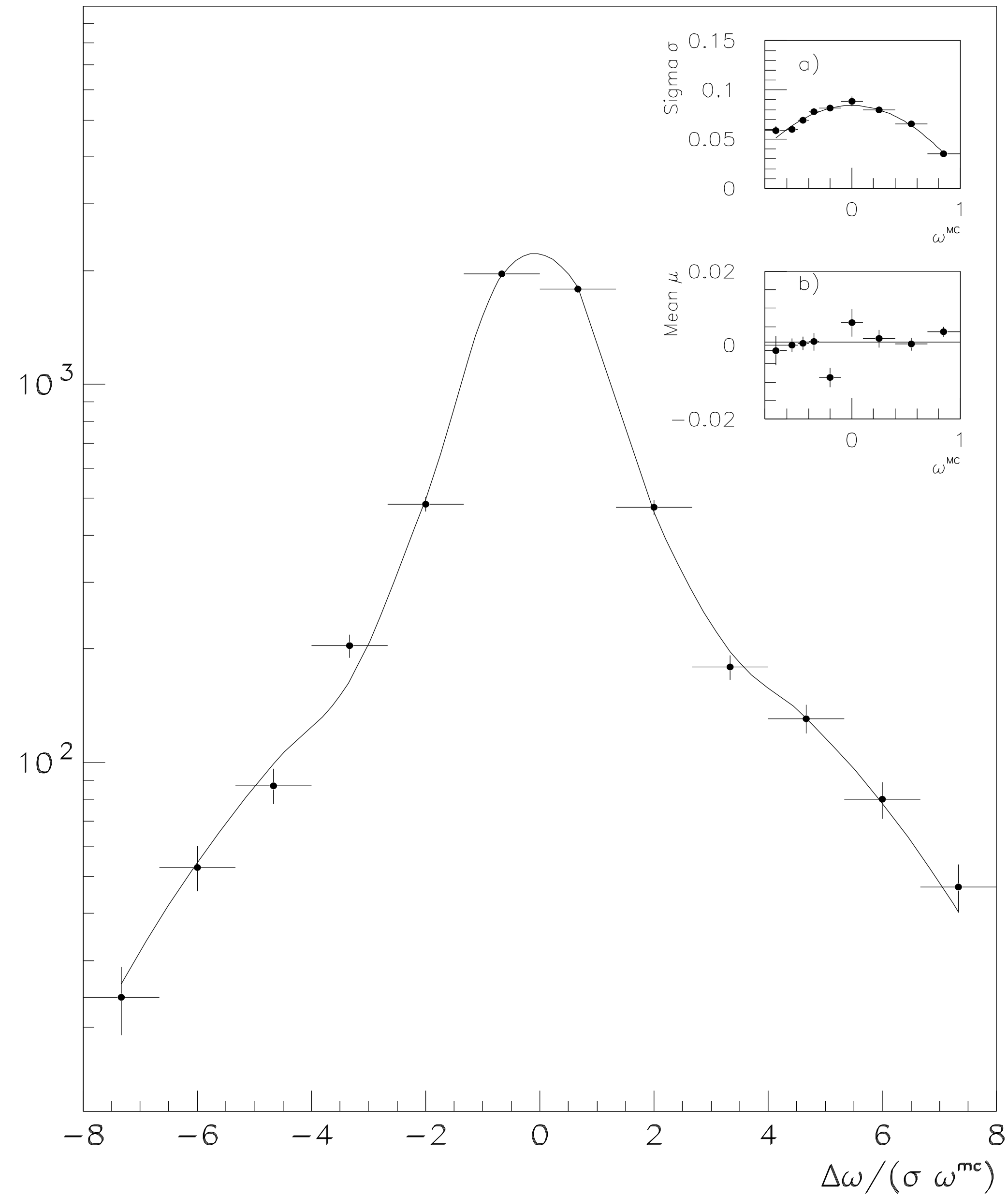

Figure 18: ω Resolution for "Right Hand enhanced" $\tau \to \rho \nu_\tau$ events.

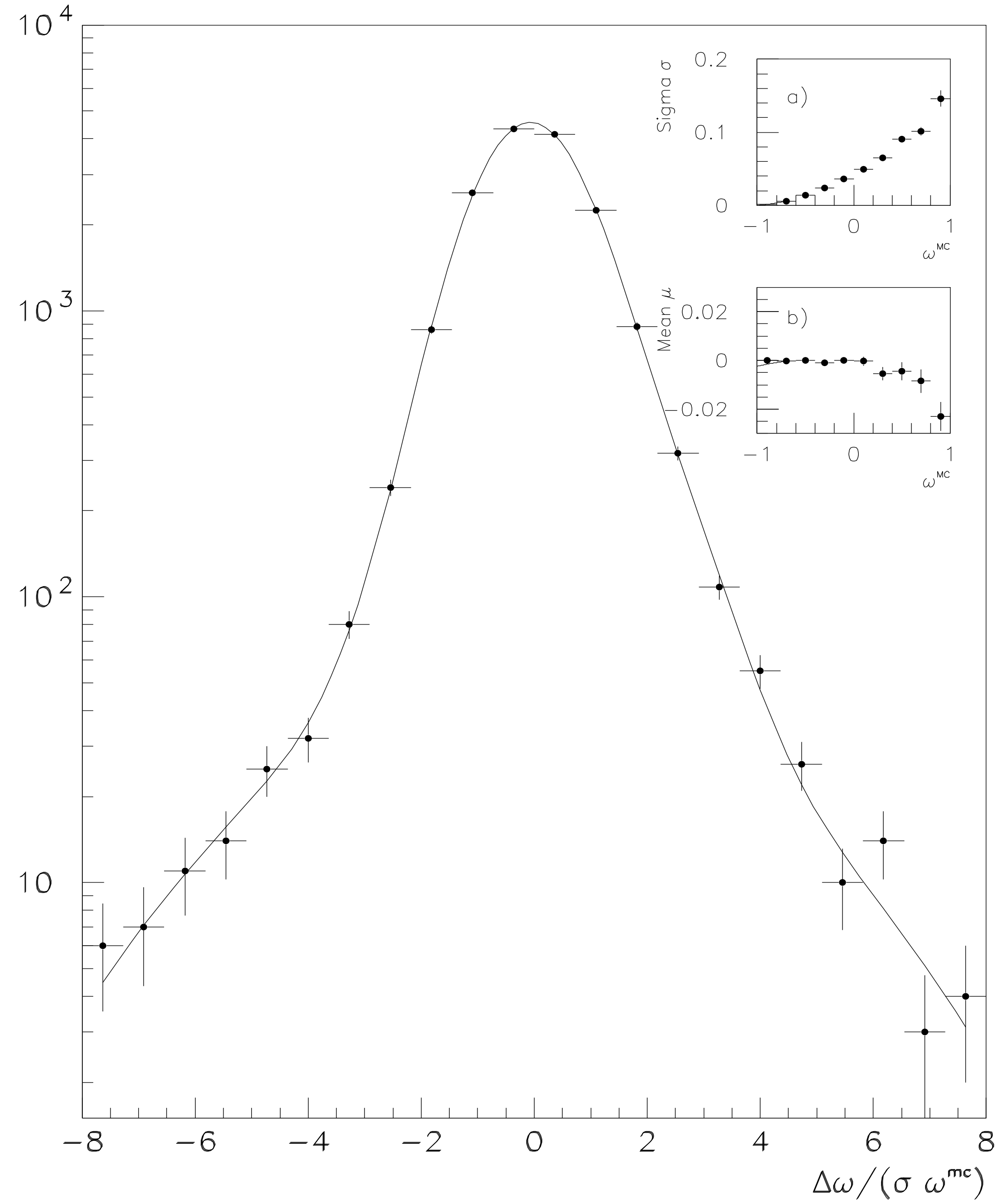

Figure 19: ω Resolution for $\tau \rightarrow \pi(\mathrm{K})\nu_\tau$ events.

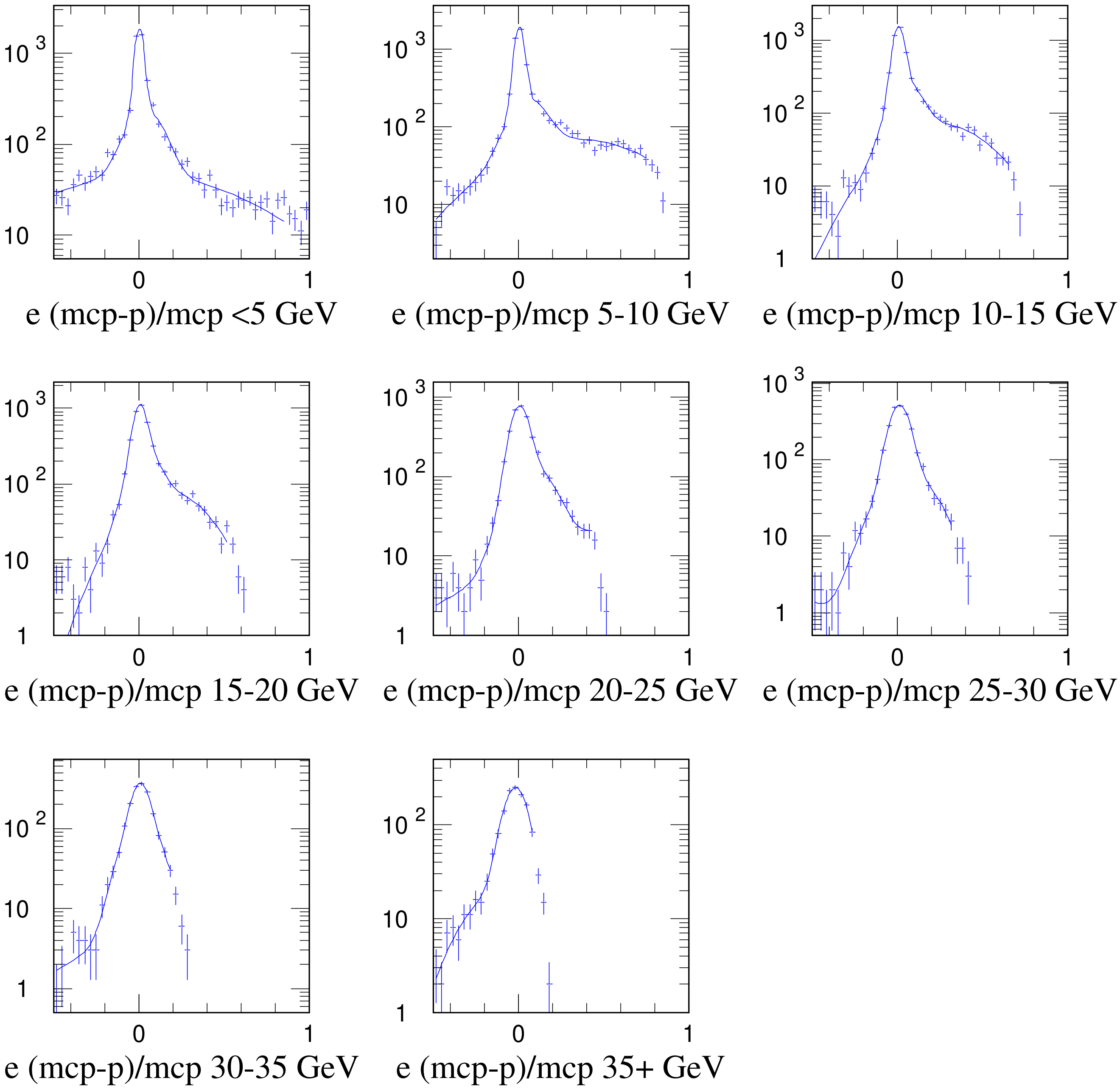

Figure 20: The electrons scaled energy resolution as parameterized in the different z regions

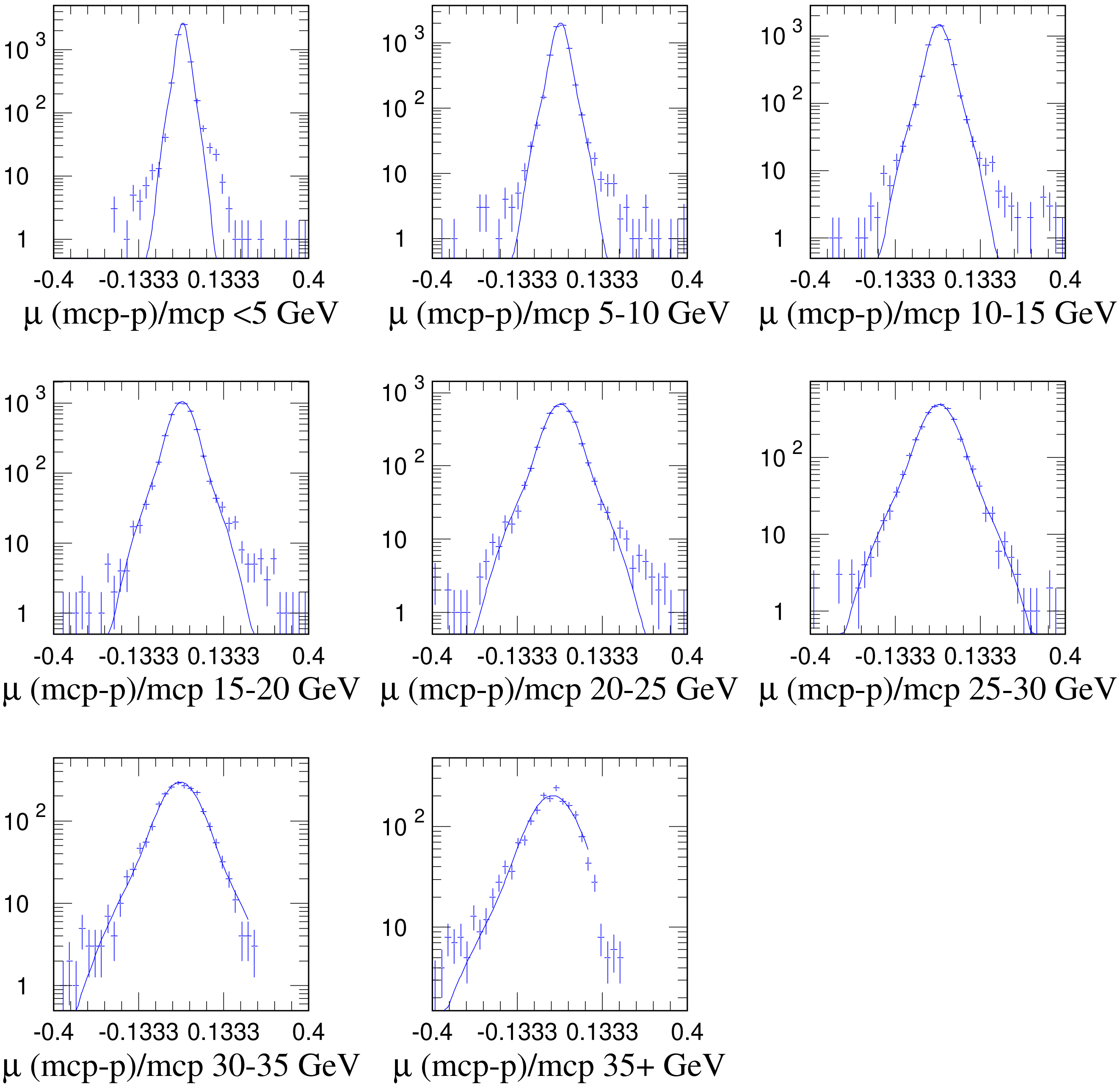

Figure 21: The muons scaled energy resolution as parameterized in the different z regions

8.3 Radiative Corrections

The radiative corrections were determined from large samples of generator level τ decays, generated with KORALZ, with initial/final state radiation turned on and off. The distribution is formed by,

$$\mathcal{R}_{RC} = \frac{Radiation - Off}{Radiation - On} \tag{16}$$

The distribution were parameterized separately as a function of $cos\theta_\tau$ and ω for the four samples consisting of each combination of positive/negative $cos\theta_\tau$ and positive/negative tau polarization, $\mathcal{P}_\tau$. This correction was applied to the theoretical function prior to convolution with the resolution function. Figs. 22-24 present the distributions used for the radiative corrections.

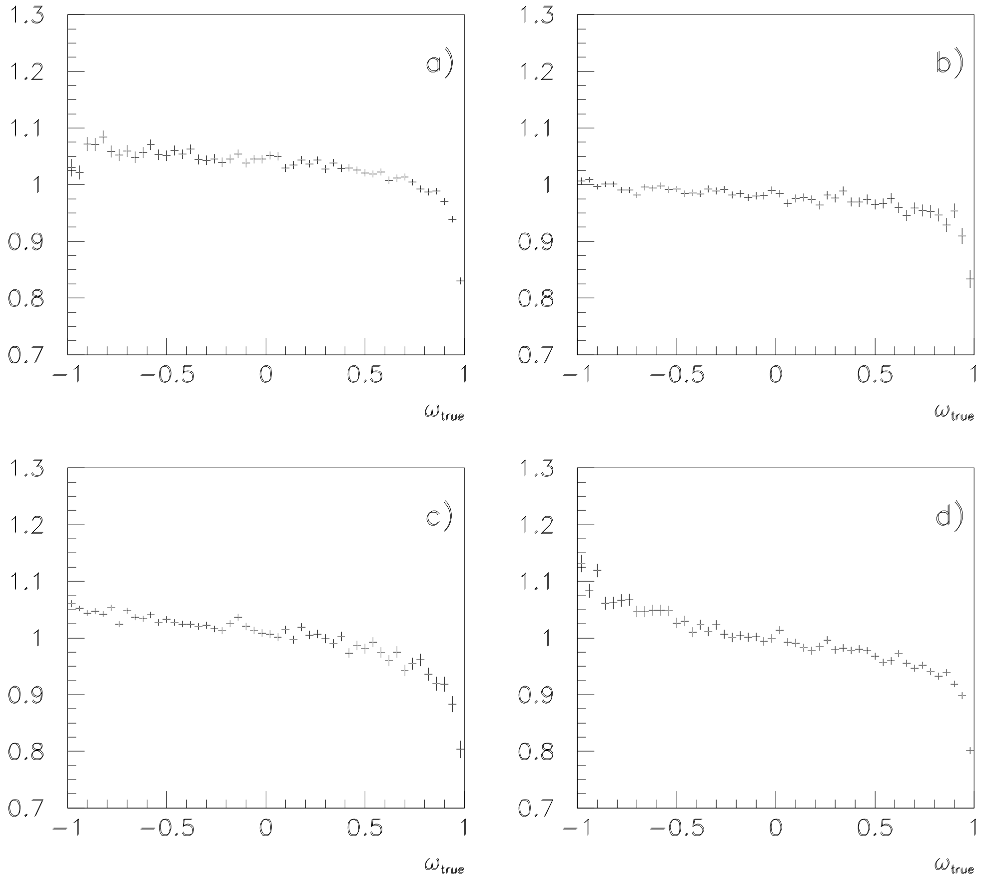

Figure 22: $\tau \rightarrow \pi(\mathrm{K})\nu_\tau$ radiative correction curves. Plots (a,b) are for left hand polarized beam, (c,d) are for right hand polarized beam. The plots of the left side are for $\cos\theta < 0$. and the plots on the right side are for $\cos\theta > 0$..

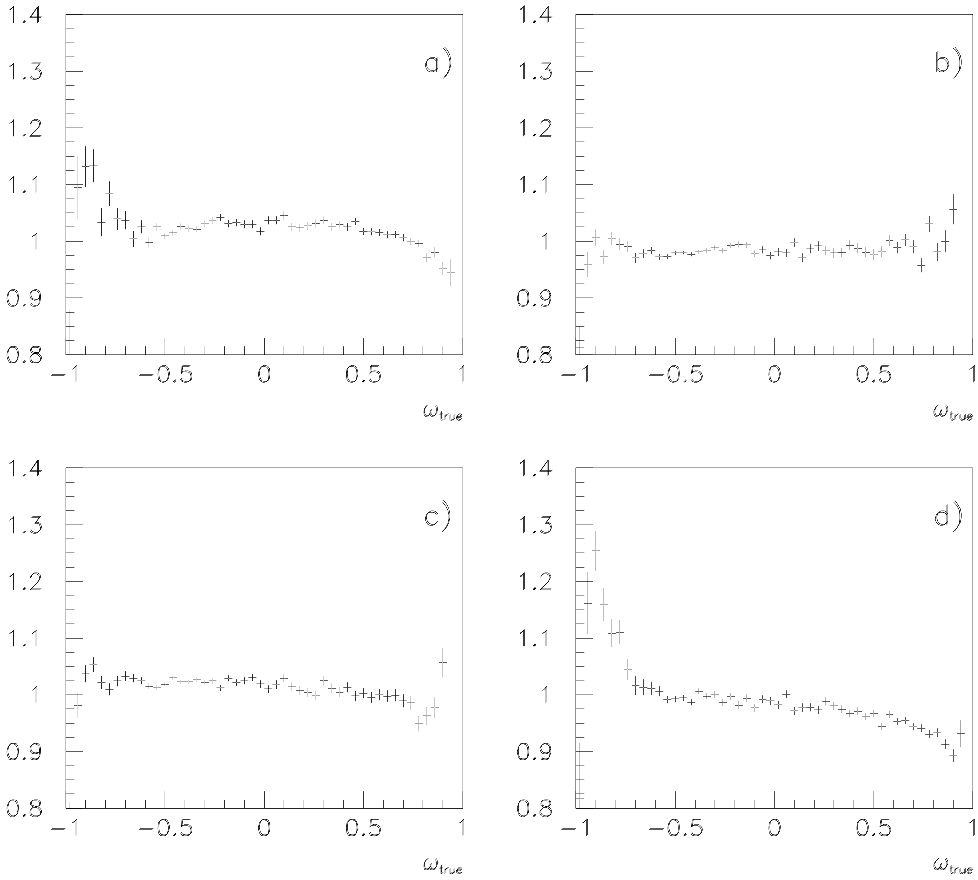

Figure 23: $\tau \rightarrow \rho\nu_\tau$ radiative correction curves. Plots (a,b) are for left hand polarized beam, (c,d) are for right hand polarized beam. The plots of the left side are for $\cos\theta < 0.$ and the plots on the right side are for $\cos\theta > 0.$.

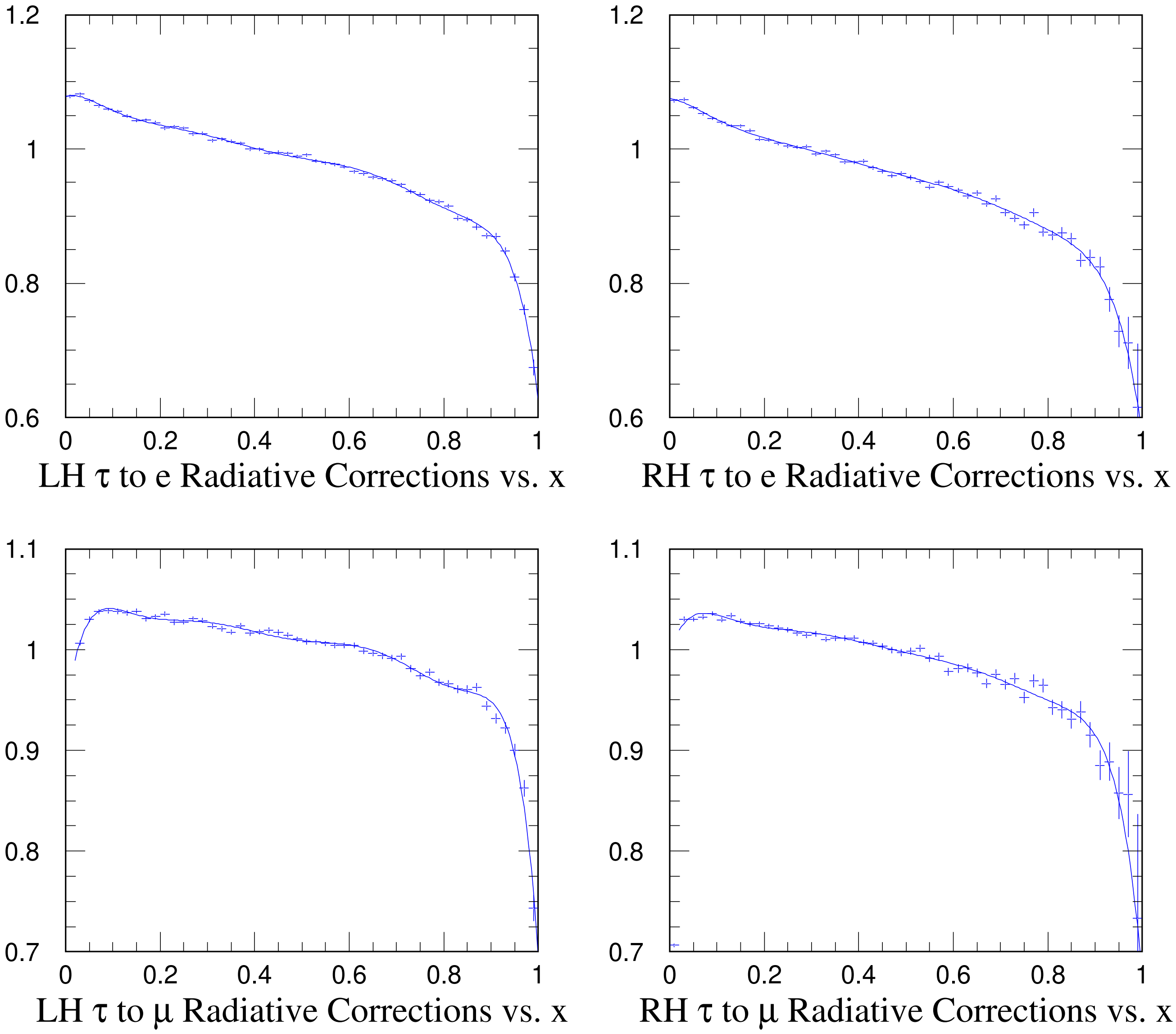

.

Figure 24: Radiative corrections for electrons (a,b) and muons (c,d). Plots (a,c) are for left hand polarized beam, (b,d) are for right hand polarized beam.